USC UNIVERSIDADE DE SANTIAGO DE COMPOSTELA
CAMPUS VIDA CAMPUS DE EXCELENCIA INTERNACIONAL
CiQUS Center for Research on Biological Chemistry and Molecular Materials

Stimuli-Directed Colorimetric Interconversion of Helical Polymers Accompanied by a Tunable Self-Assembly Process

Rafael Rodríguez, Emilio Quiñoá, Ricardo Riguera, Félix Freire

Peer reviewed version

This is the peer reviewed version of the following article: Rodríguez, R., Quiñoá, E., Riguera, R., Freire, F., Small 2019, 15, 1805413, which has been published in final form at https://doi.org/10.1002/smll.201805413. This article may be used for non-commercial purposes in accordance with Wiley Terms and Conditions for Use of Self-Archived Versions

How to cite:

Rodríguez, R., Quiñoá, E., Riguera, R., Freire, F., Small 2019, 15, 1805413. https://doi.org/10.1002/smll.201805413

Copyright information:

© 2019 WILEY-VCH Verlag GmbH & Co. KGaA, Weinheim. This article may be used for non-commercial purposes in accordance with Wiley Terms and Conditions for Use of Self-Archived Versions

Stimuli-Directed Colorimetric Interconversion of Helical Polymers accompanied by a Tunable Self-Assembly Process

Rafael Rodríguez, Emilio Quiñoá, Ricardo Riguera and Félix Freire**

R. Rodríguez, Prof. E. Quiñoá, Prof. R. Riguera, Prof. F. Freire
Centro Singular de investigación en Química Biolóxica e Materiais Moleculares (CiQUS) and Departamento de Química Orgánica, Universidade de Santiago de Compostela, E-15782 Santiago de Compostela, Spain.
E-mail: felix.freire@usc.es, ricardo.riguera@usc.es

Keywords: helical polymer, gel, colorimetric sensor, self-assembly, poly(phenylacetylene)

Interconversion between extended and bent structures at the pendant groups of a chiral polyene framework [poly(phenylacetylene) with (*R*)-(2-methoxy-2-phenylacetyl)glycine residues linked to 4-vinylanilines] allows the reversible colorimetric transformation from stretched to compressed helical cis-transoid polyenic structures through manipulation of the flexible spacer. This transformation generates either organogels (stretched helical form) or nanoparticles (compressed helical form) under the control of polar/low polar stimuli respectively and opens the way to the development of new sensors and stimuli-sensitive materials based on these concepts.

1. Introduction

Dynamic helical polymers, such as poly(phenylacetylene)s (PPAs), [1] are very interesting macromolecules largely due to their stimuli-responsive properties. Their helical sense and elongation can be manipulated by the action of external stimuli such as chiral additives, polarity changes or metal ions. [2] Thus, these materials can act as sensors, [3] chiroptical switches, [4] chiral stationary phases [5] or chiral catalysts, [6] among other applications.

Chiral PPAs usually establish equilibrium between the two helical senses (*P* or *M*) of the polyene backbone, and this equilibrium is biased depending on the conformational composition of the pendant. [2] It is well known that inversion of the helical sense is possible by altering the conformation of the chiral pendants. [7] In some cases, this helical inversion is

accompanied by a change in the elongation of the polyene chain detected by CD or UV spectroscopies (bathochromic or hypsochromic shifts). [3, 7, 8]

It is also known that changes on the elongation of the polymer can be accompanied by colorimetric changes, although the parameters or mechanism that govern these stretching or compression fluctuations in the polymer still remain unclear. [9]

Our group has recently reported a PPA that shows chiral teleinduction from a remote chiral center due to the presence of a well-folded β-sheet structure of Gly residues acting as flexible spacer. [4]

Herein, we want to make a step forward in the study of stimuli-responsive helical polymers [10] by acting selectively on the flexible fragment at the pendant group made by an achiral extensor and a chiral center (**Scheme 1**). This kind of helical sense control has not been explored to date, being usually the chiral moiety of a PPA the one affected by the presence of different external stimuli.

Further manipulation of a flexible spacer in a PPA should result additionally in an elongation change of the PPA. Thus, the helical scaffold could be switched from a helical compressed structure towards highly stretched one (**Scheme 1**).

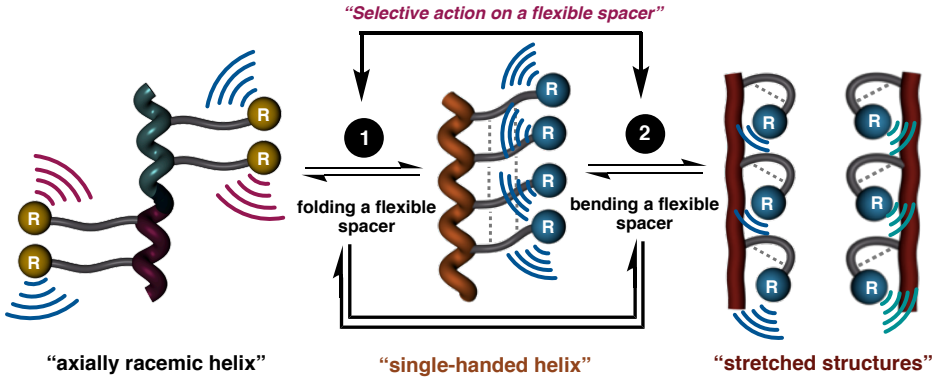

Scheme 1. Conceptual illustration of three different states adopted by a PPA by selective actuation on a flexible spacer.

To achieve this goal, it is necessary to design a pendant group capable to produce a controllable and reversible large steric hindrance on the helical scaffold by the presence of an

external stimulus. Thus, once generated a congested structure, the strain will be released by twisting the conformation of the ω_1 bond (C=C—C=C) up to extreme angular values (i.e., close to 180º), thus forcing the polyenic chain to adopt an almost fully conjugated, planar structure.

The presence of both stretched and compressed helical scaffolds in equilibrium is interesting from both structural and applied points of view. While planar polymeric structures are particularly appealing because of the optical, conductive and electrical properties associated to the conjugation, [11] poorly conjugated helical polymers have found successful applications as chiral materials in different fields as stated before. [3, 6]

Therefore, in this paper we describe a PPA aimed to fulfill such a requirement: the existence of equilibrium between helical and flat structures, which responds to an external stimulus (i.e., polarity) by the reversible conversion of its helical compressed structure into a stretched, almost planar one and *vice versa.* Moreover, the helical structure can appear folded into a predominant one-handed helix or as a macroscopically racemic helix depending on how well organized the flexible spacer is.

So, in order to proceed to its design, we took into consideration that the elongation degree of a helical PPA (easily detected by CD and UV) is related to the steric hindrance of the pendant group attached to the phenyl ring: PPAs with large substituents tend to adopt more extended helices than those with smaller ones and polymers with the substituents in *ortho* have more elongated helices than those with the same group in *meta* or *para.* [12]

With these ideas in mind, we devised a pendant group that adopts equilibrium between two interconvertible linear and bent structures. This pendant can be a flexible peptide mimetic fragment showing equilibrium between three different structural motifs: 1) a linear β-sheet stabilized by an interpendant hydrogen bond network, 2) a bent structure stabilized by intrapendant H-bonds, and 3) an unfolded structure (Scheme 1). [13]

Thus, while the unfolded flexible pendant group undergoes to the formation of an axially racemic helix (null CD), the β-sheet like orientation of the pendants should produce a predominant one-handed compressed helix if effective chiral teleinduction is transmitted from the remote chiral center to the polyene backbone. On the other hand, the helical structure that bears the congested bent structure at the pendant should be associated to a more elongated polymeric form. Cleavage/formation of the different hydrogen bond networks should be enough to trigger the conversion from the axially racemic (no H-bond network) to a predominant one-handed and compressed helix (parallel β-sheet) to finally evolve towards a highly stretched axially racemic helix and *vice versa* (Scheme 1).

2. Results and Discussion

This idea can be materialized by a pendant formed by a glycine unit —bonded as anilide to the polyenic backbone— which is *N*-bonded to a chiral α-methoxy-α-phenylacetic acid (MPA) unit (Figure 1a). [14]

The “extended/bent" equilibrium will be dictated by the presence of either a hydrogen bond network between amide bonds of the n and n+2th neighboring pendants groups, or a hydrogen bond between the acidic NH of the anilide and the terminal amide carbonyl. Those hydrogen bond arrays should be tunable by solvents of appropriate characteristics (**Figure 1a**).

In the open extended form, there is no much steric hindrance among pendants, and the chiral MPA units will induce a preferred helical sense in the backbone through chiral teleinduction.

However, in the bent form, the MPA moieties will produce steric hindrances, large enough to force the backbone to abandon the compressed helical structure towards a highly stretched one.

Interconversion between the stretched and the compressed helical structures will be obtained by acting on the different hydrogen bond networks at the pendant groups through thermal treatment.

Hence, the glycine residue, although achiral, becomes a key factor defining the helical structure adopted by the polymer. Its conformational flexibility will either arrange the pendant groups into a β-sheet like or into a bent structure, resulting in the formation of two different structures of the polyene backbone, one helical and another planar structures.

Thus, to test our hypothesis we prepared the 4-ethynylanilide of the H-Gly-(*R*)-MPA (m-**1**) (Figure 1). Different structural studies were carried out in m-**1** to determine the presence of equilibrium between a linear and a bent structure. X-ray studies shown that the monomeric unit adopts a preferred linear orientation for the Gly-(*R*)-MPA fragment, which evidence the possible adoption of a β-sheet like orientation at the pendant moiety within the PPA (Figure 1b).

CD studies in polar and low polar solvents revealed the presence of a major antiperiplanar (*ap*) conformation in the MPA final fragment [15] (see Figure S5). Thus, in this case polarity does not affect the MPA conformational equilibrium, and therefore the chiral part of the pendant group is fixed into a specific conformation in the different polar and non-polar solvents.

However, NMR studies in in polar and low polar solvents shown large differences. The proton NMR signals of the 4-ethynylanilide group (alkyne, NH and aromatic) suffer a dramatic upfield shifting when going from polar to low polar solvents. The orientation of the aryl rings justifies the upfield shifting of the ethynylanilide group —alkyne, aromatic and amide protons— (see Figure 1b). Therefore, these results strongly suggest the presence of a major bent structure in low polar solvents and a linear one in polar solvents. To further verify these results, VT and concentration dependence experiments were carried out next.

VT-NMR experiments for m-**1** in low polar solvent (1mg/mL $CHCl_3$), confirmed the presence of a major bent structure. Thus, it was found that when temperature decreases, the amide proton of the anilide suffers a strong low field shifting effect (1 ppm), which indicates the presence of a hydrogen bond interaction between this NH and the carbonyl of the Gly residue,

only present in the bent conformation (Figure 1c). In addition, the two protons of the Gly become more diastereotopic at lower temperature due to the different anisotropic environment generated in the bent form of m-**1** (Figure 1c). Furthermore, the upfield shifting observed in the aromatic protons of the anilide group when the temperature decreases are again in agreement with the presence of a bent structure —the aromatic ring of the MPA moiety faces the anilide group— (Figure 1b and c).

Finally, the amide proton of the Gly is also downfield shifted (<0.4 ppm), most likely due to a further stabilization of the most stable MPA *ap* conformation that increases its interaction with the methoxy group. [16]

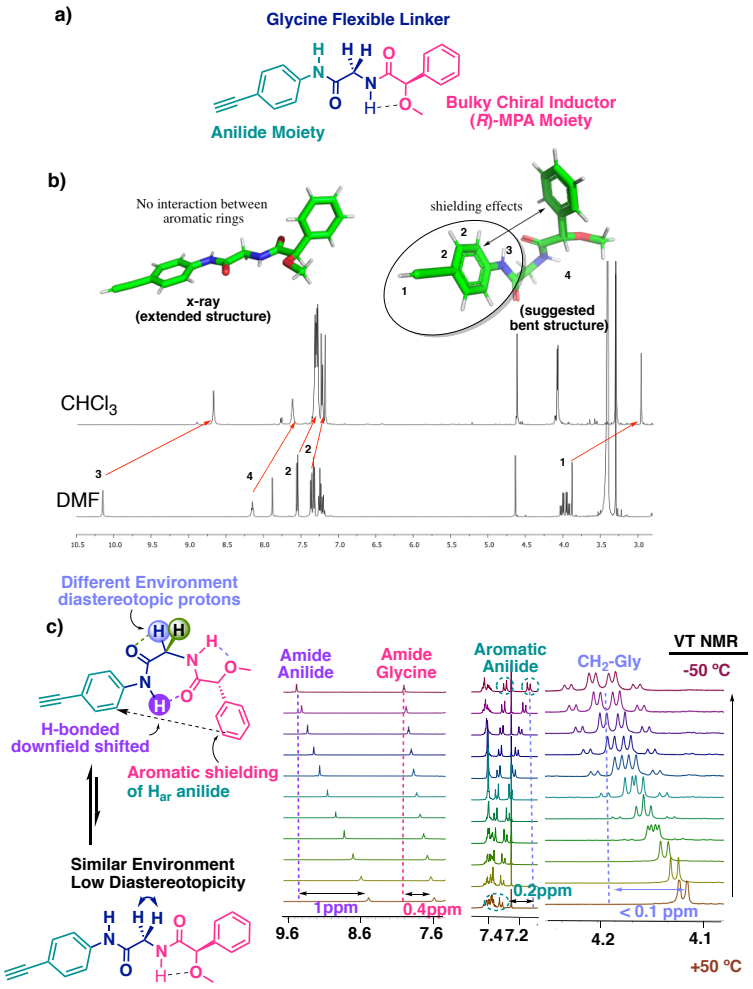

Figure 1. a) Chemical structure of monomer 1. b) 3D models showing the relative position of the aromatic rings in the extended (X-ray) and the bent conformations of m-**1**. The shifts

observed in NMR spectra (below) support the presence of these two different conformations.

c) ^{1}H VT-NMR of monomer **1** in chloroform. [m-**1**]= 1mg/mL.

VT experiments were also carried out in polar solvents (1mg/ mL DMF) and indicate the presence of an extended structure for the Gly-MPA fragment. The two-amide groups suffer downfield shifting when temperature decreases due to interaction with the polar solvent, while the two-methylene protons of the Gly residue and the aromatic protons of the anilide group remain almost identical in all the range of temperatures. This result indicates that the beta-sheet conformation is the preferred one in polar solvents for monomer **1** (Figure S7).

In order to confirm the presence of this equilibrium and avoid possible aggregation effects, different ^{1}H NMR spectra were collected at different concentrations in both polar (DMF) and low polar solvents ($CHCl_3$). In these experiments, movements associated to the presence of supramolecular aggregates were only observed in the amide protons —no chemical shift deviations observed for the alkyne or the aromatic protons of the 4-ethynylanilide group— (Figure S6).

Therefore, from these experiments we can extract that although supramolecular interactions can occur at high monomer concentrations, the NMR spectra of these aggregates are different to the one associated to an extended/bent conformational equilibrium at m-**1**.

Next, monomer **1** was polymerized with $[Rh(nbd)Cl]_2$ (nbd= 2,5-norbornadiene) as catalyst in THF in the presence of triethylamine in a similar way to that previously reported,[2a-b] obtaining poly-**1** in high yield and with high *cis* content of double bonds (**Figure 2a**). The number-average molecular weight (*M*n) and its distribution (*M*w/*M*n) were estimated to be 1.9 $\times 10^4$ and 1.2 respectively as determined by size exclusion chromatography (SEC).

CD and UV experiments of poly-**1** in different solvents suggest the presence of two different polymer scaffolds.

Thus, while poly-**1** dissolved in polar solvent (i.e., TFE) is light yellow (i.e., "yellow" form) and shows a CD trace typical for a PPA with a predominant helical sense (negative Cotton effect at the vinylic region, UV absorbance for the polyene backbone λ= 410 nm, Figure 2b, Figure 2d), in low-polar solvents (i.e., DCM, $CHCl_3$ and THF, Figure 2c and Figure 2d) the polymer solution shows an intense red color (i.e., "red" form), with a null CD in the polyene region, and where this polyene maximum absorbance is red shifted at λ= 530 nm. This large bathochromic effect (from λ= 410 nm to λ= 530 nm, Figure 1c) is associated to the presence of a mixture of *P* and *M* highly stretched helical structures.

This result in combination with the data obtained from CD —no signal on the vinylic region—, DSC —isomerization bands shifted towards higher temperature (see Figure 3f and 3g)—, and Raman spectroscopy —polyene Raman resonance bands moved towards lower frequencies [*cis*- C-H band appears in DMSO at values typical for a *c-t* structure (i.e., 1003 cm^{-1}, see Figure 3h*)* [11] while in $CHCl_3$ (red form) this *cis*- C-H band appears now at 966 cm^{-1} indicating a more stretched *c-t* skeleton (See Figure 3i)]— suggests the presence of a highly conjugated and almost planar polyenic backbone.

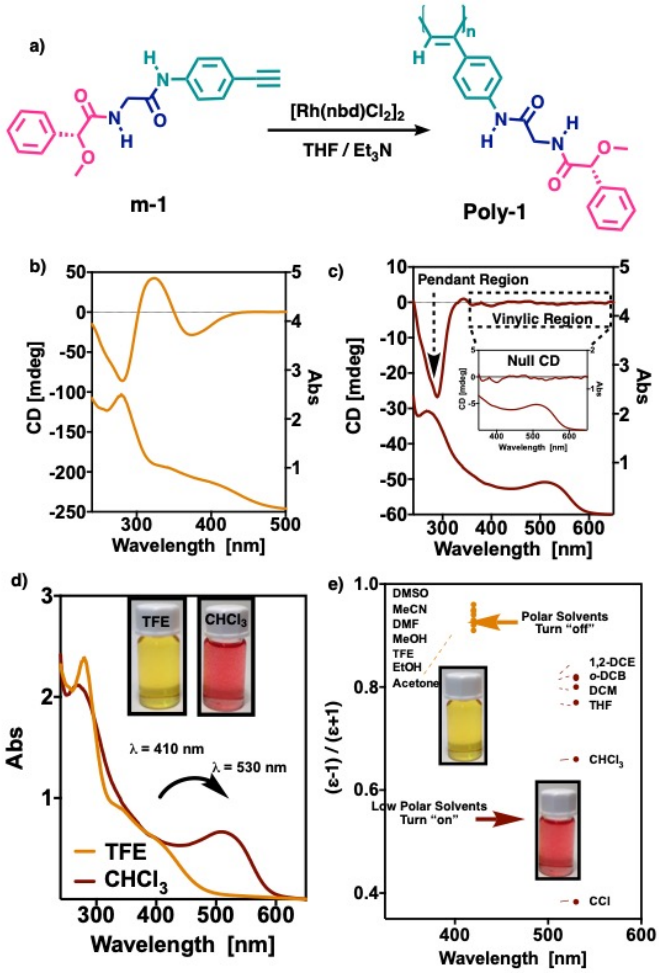

Figure 2. a) Synthesis of poly-**1**. b) Representative CD/UV spectra of poly-**1** in polar solvents (e.g., TFE, 0.5 mg/mL). c) Representative CD/UV spectra of poly-**1** in low polar solvents, inset graph highlighting the null CD in the vinylic region (e.g., $CHCl_3$, 0.5 mg/mL). d) Overlay of UV spectra of poly-**1** in $CHCl_3$ and TFE (0.5 mg/mL). e) Plot of the maximum UV absorption of poly-**1** skeleton as function of the polarity of different solvents (see Ref. 11). DSC trace of poly-**1** annealed in (f) polar and (g) low polar solvents. Raman spectra of poly-1 in the helical state. Raman spectra of poly-**1** annealed in (h) polar and (i) low polar solvents.

NMR experiments of poly-**1** in different solvents corroborate the elongation of the polyene backbone in low polar solvents; the vinyl proton in $CHCl_3$ did not resonate in the region typical for helical structures (5.6-5.8 ppm) but resonates very downfield (6-8 ppm) compatible with a highly stretched helical structure (see Figure S8 and S9 for further explanation). In

addition, the methylene protons of the glycine residue resonate with different diastereotopicity in both helical structures (compressed/stretched) (Figure S8b), suggesting the presence of different conformations for the pendant in both helical scaffolds, in a similar manner to the monomeric form. Thus, the pendant adopts an extended β-sheet orientation in polar solvent, while a bent conformation is adopted in low polar solvents. The poor solubility of the polymer in the low polar solvent, and the presence of an intense CD signal at 290 nm, suggest the presence of stereoregular almost flat structure, where the pendant group is still well organized into an antiperiplanar conformation between the carbonyl and the methoxy groups at the MPA moiety.

The interconversion between a compressed and a stretched helical structure is a reversible process, being possible to interconvert a compressed helix into an extended one and vice versa (See Figure S12e-f).

With all the aforementioned information in hand, we built tentative 3D-models of poly-**1** adopting both *c-t* compressed and stretched helical structures. In the case of the compressed helical form adopted by poly-**1** in polar solvents, a left-handed helix is described by the polyene backbone (ω_1>90), and according to this, a right-handed helix must be described by the pendants. [16] The helical structure is stabilized by intramolecular hydrogen bonding between n^{th} and $n+2^{th}$ pendants forming a parallel β-sheet structure that now promotes the harvesting of the chiral information of the MPA moiety by the polyene backbone (**Figure 3a**). [4]

On the other hand, when poly-**1** is dissolved in low polar solvents, an almost planar, highly conjugated structure is formed.

This structure should have a ω_1 angle in the polyene backbone close to 180º, which can be either positive or negative resulting in a highly conjugated axially racemic structure, which is

stabilized by the "crowded" bent structure present in the pendants. As a consequence, the pendants along this linear axis are also arranged in an almost linear array (Figure 3b).

These two different structures adopted by poly-**1** in polar and low polar solvents can clearly explain their different solubility. Thus, poly-**1** in polar solvents adopts a helical structure, and shows good solubility (Figure 3a), due to the lack of possible supramolecular interactions between helices.

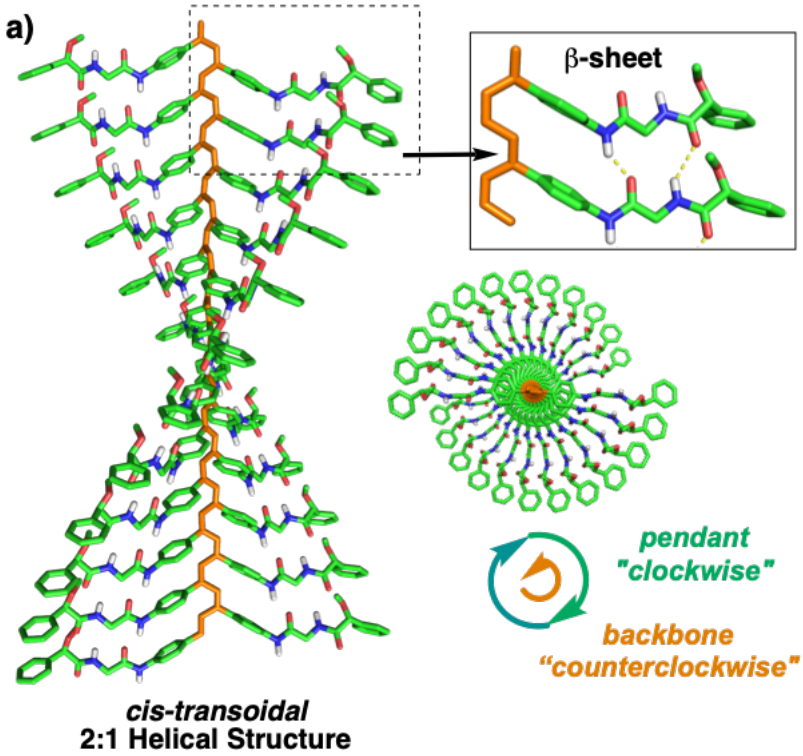

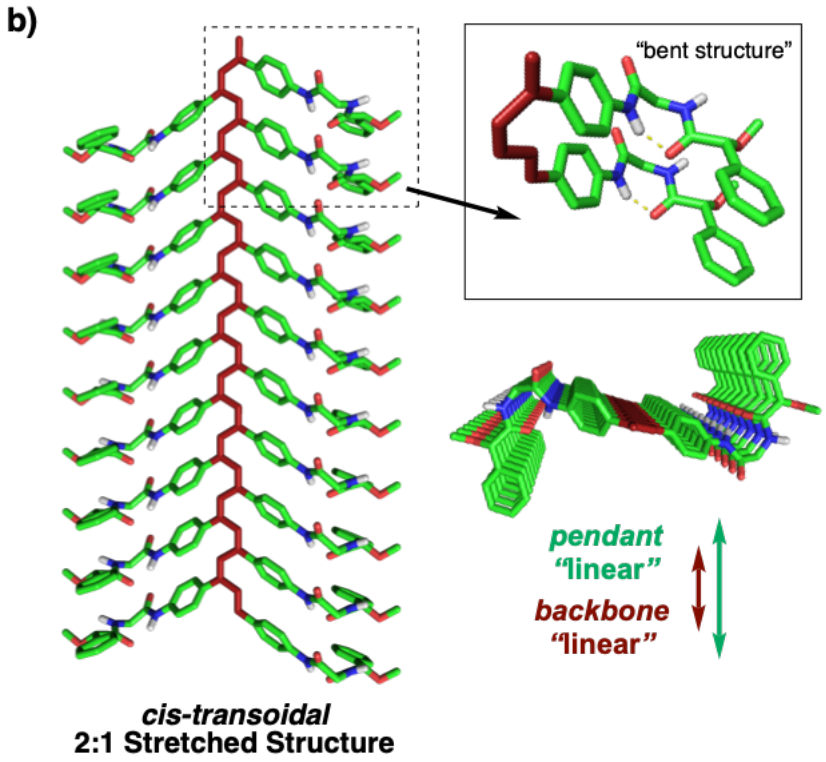

Figure 3. Conceptual representation of the helical structures adopted by poly-**1** in (a) polar and (b) low polar solvents.

On the contrary in low polar solvents, this material shows poor solubility and a high tendency to aggregate. [12] Looking at the almost planar structure postulated for poly-**1** in low polar solvents (**Figure 4a**), we could observe how the amide groups are exposed to the outer part of the polymer structure. Amide groups from different polymer chains can interact through supramolecular hydrogen bond interactions forming an amide zipper motif, which can linearly interlock different polymer chains (Figure 4b). Moreover, this aggregate can also grow in a 3D way due to hydrophobic interactions between the quasi-planar and highly hydrophobic skeleton of a polymer chain with the aromatic rings of the MPA unit of a different polymer chain (Figure 4c).

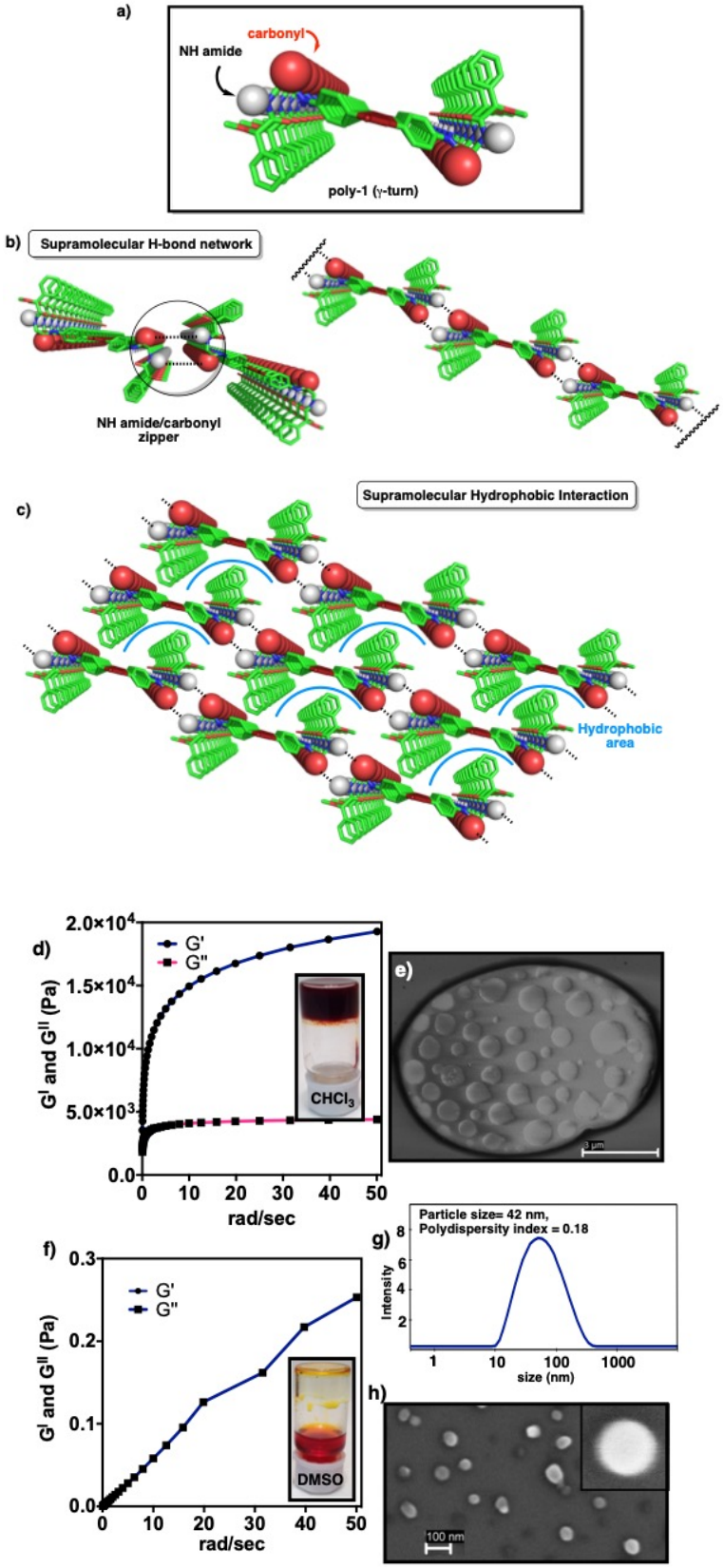

Figure 4. a) Conceptual representation of the highly stretched structure adopted by poly-**1** in low polar solvents. b) Schematic representation of the amide zipper interlocking different poly-1 chains. c) 3D aggregate for poly-**1** due to supramolecular amide interactions and

hydrophobic effects. d) Rheology experiment of poly-**1** ($CHCl_3$, 40 mg/mL) and inset picture of the macroscopic gel formed. e) SEM image of the gel. f) Rheology experiment of poly-**1** (DMSO, 40 mg/mL) and inset picture of the viscous solution obtained. g) DLS trace of poly-**1** (DMSO, 0.1 mg/mL) showing the presence of polymer nanoparticles in solution with size around 40 nm. h) SEM images of the polymeric nanoparticles (DMSO, 0.1 mg/mL).

In fact, a well-characterized organogel[17] is formed at concentrations above 10 mg/mL in $CHCl_3$ (see Figure 4d-e, Figure S15 and Figure S17 for AFM and SEM studies).

On the contrary, the yellow helical form adopted by poly-**1** in polar solvents is soluble up to 100 mg/mL in DMSO. Rheology measurements showed that at around 40 mg/ml, a viscous solution appears but still without signs of gelation (Figure 4f).

Moreover, DLS of this yellow sample showed the presence of small polymeric nanoparticles (40 nm, PDI= 0.18, Figure 4g), whose spherical shape and size were confirmed by SEM (Figure 4h and Figure S16).

Finally, both the extended and the compressed helices can be transformed into a compressed axially racemic helix by heating. The different hydrogen networks, which stabilize both structures, are disrupted, transforming the well-oriented spacer into a flexible one. As a result, chiral teleinduction is lost in polar solvents; while in low polar solvents the planar structure is the one that disappear, changing the color solution from red to yellow (see Figure S12c).

Analogous studies were carried out for the enantiomeric form of poly-(*R*)-**1** —i.e., poly-(*S*)-**1**— and as expected and due to their enantiomeric relationship, mirror image CD traces were obtained for both polymers in the different solvents (Figure S21). Moreover, both polymers show the same aggregation tendency in low polar solvents.

3. Conclusion

In conclusion, introduction of an interconvertible bent/extended structural motif in the pendants of a poly(phenylacetylene) allows the polymer to switch from a predominant one-handed helix induced through chiral teleinduction to a quasi-planar helical structure *and vice versa* by the presence of an external stimuli. This strategy opens a new way to the development of new sensors and stimuli responsive materials based on this type of behavior.

In helical polymers, to enhance or invert the helical structure adopted by the polymer is necessary to play with the conformational composition of the chiral moiety. Herein, we show how manipulating the conformational composition of an achiral spacer it is possible, not only to activate/deactivate the chiral teleinduction commanded from a remote chiral fragment, but also to modulate drastically the 3D structure adopted by the polymer, *i.e.* from helical to planar or vice versa which is in our case accompanied by a color change of the solution.

The extended/bent equilibrium of the pendant group was demonstrated in the monomer unit (RMN), and is clearly evidenced in poly-**1,** by the two completely different scaffolds adopted in polar and low polar solvents characterized by CD, UV, ^{1}H-NMR, DSC and Raman.

The presence of a bent structure at the pendant moiety in combination with the presence of a highly stretched helical structure for the polyphenylacetylene backbone results in a polymer scaffold with a large tendency to aggregate due to interlocking of polymer chains through an amide zipper and hydrophobic interactions.

Thus, reversible organogels are formed in low-polar solvents (stretched helical form) while polymer particles are obtained in polar solvents (compressed helical form).

Supporting Information

Supporting Information is available from the Wiley Online Library or from the author.

Acknowledgements

Financial support from MINECO (CTQ2014-61470-EXP, CTQ2015-70519-P), Xunta de Galicia (GRC2014/040, Centro singular de investigación de Galicia accreditation 2016-2019,

ED431G/09) and the European Regional Development Fund (ERDF) is gratefully acknowledged. R. R. is grateful to MINECO for a FPI predoctoral fellowship. We also thank Prof. Dr. Carmen Álvarez-Lorenzo (Dept. Farmacia y Tecnología Farmaceútica, Facultad de Farmacia, USC) for invaluable assistance in the rheology studies, and Servicio de Microscopía Electrónica (CACTUS, USC).

Received: ((will be filled in by the editorial staff))
Revised: ((will be filled in by the editorial staff))
Published online: ((will be filled in by the editorial staff))

References

[1] a) F. Freire, E. Quiñoá, R. Riguera, *Chem. Commun.* 2017, **53**, 481; b) F. Freire, E. Quiñoá, R. Riguera, *Chem. Rev.,* 2016, **116**, 1242; c) E. Yashima, N. Ousaka, D. Taura, K. Shimomura, T. Ikai, K. Maeda, *Chem. Rev.*, 2016, **116**, 13752. d) E. Yashima, K. Maeda, H. Iida, Y. Furusho, K. Nagai, *Chem. Rev.,* 2009, **109**, 6102; e) J. Liu, J. W. Y. Lam, B. Z. Tang, *Chem. Rev.,* 2009, **109**, 5799.

[2] a) F. Freire, J. M. Seco, E. Quiñoá and R. Riguera, *J. Am. Chem. Soc.*, 2012, **134**, 19374; b) F. Freire, J. M. Seco, E. Quiñoá, R. Riguera, *Angew. Chem. Int. Ed.*, 2011, **50**, 11692; c) E. Yashima, K. Maeda, Y. Okamoto, *Nature,* **1999**, 399, 449.

[3] a) E. Anger, H. Iida, T. Yamaguchi, K. Hayashi, D. Kumano, J. Crassous, N. Vanthuyne, C. Rousselc, E. Yashima, *Polym. Chem.* **2014**, *5*, 4909. b) H. Iida, M. Miki, S. Iwahana, E. Yashima, *Chem. Eur. J.* **2014**, *20*, 4257. c) S. Leiras, F. Freire, J. M. Seco, E. Quiñoá, R. Riguera, *Chem. Sci*. **2013**, *4*, 2735. d) S. Sakurai, K. Okoshi, J. Kumaki, E. Yashima, *J. Am. Chem. Soc.* **2006**, *128*, 5650.

[4] R. Rodriguez, E. Quiñoá, R. Riguera, F. Freire, *Chem Mat*. **2018**, *30*, 2493.

[5] K. Shimomura, T. Ikai, S. Kanoh, E. Yashima, K. Maeda. *Nat. Chem.*, **2014,** 6, 429.

[6] a) H. Iida, Z. Tang, E. Yashima, *J. Polym. Sci., Part A: Polym. Chem.* **2013**, *51*, 2869; b) Z. Tang, H. Iida, H.Y. Hu, E. Yashima, *ACS Macro Lett.* **2012**, *1*, 261; c) R. P. Megens, G. Roelfes, Asymmetric Catalysis with Helical Polymers. *Chem. Eur. J.* **2011**, *17*, 8514; d) X. Liu, L. Lin, X. Feng, *Acc. Chem. Res.*, **2011**, *44*, 574; e) H. Iida, E. Yashima, Synthesis and Application of Helical Polymers with Macromolecular Helicity Memory, in Polymeric Chiral Catalyst Design and Chiral Polymer Synthesis, ed. Itsuno, S., John Wiley & Sons, Hoboken, NJ, USA, **2011**, ch. 7, p 201.

[7] a) M. Alzubi, S. Arias, I. louzao, E. Quiñoá, R. Riguera, F. Freire, *Chem. Commun.* **2017**, 8573; b) I. Louzao, J. M. Seco, E. Quiñoá, R. Riguera, *Angew. Chem*. *Int. Ed.* **2010**, *49*, 1430; c) S. Sakurai, K. Okoshi, J. Kumaki, E. Yashima, *Angew. Chem. Int. Ed.* **2006**, 45, 1245.

[8] a) S. Leiras, F. Freire, J. M. Seco, E. Quiñoá, R. Riguera, *Chem. Sci.;* **2013**, *4*, 2735; b) E. Yashima, K. Maeda, O. Sato, *J. Am. Chem Soc.*, **2001**, *123*, 8159.

[9] a) F. Ishiwari, K. Nakazono, Y. Koyama, T. Takata, *Angew. Chem. Int. Ed.* **2017**, *56*, 14858; b) N. Zhu, K. Nakazono, T. Takata, *Chem. Commun.* **2016**, *52*, 3647; c) F. Ishiwari, K. Nakazono, Y. Koyama, T. Takata, *Chem. Commun.* **2011**, *47*, 11739; d) K. Maeda, H. Mochizuki, K. Osato, E. Yashima, *Macromolecules* **2011**, *44*, 3217; e) K. Maeda, N. Kamiya, E. Yashima, *Chem. Eur. J.* **2004**, *10*, 4000.

[10] [10] a) S. Q. Zhao, G. Hu, X. H. Xu, S. M. Kang, N. Liu, Z. Q. Wu, *ACS Macro Lett*., **2018**, *7*, 1073-1079. b) Q. Wang, B. F. Chu, J. H. Chu, N. Liu, Z. Q. Wu, *ACS Macro Lett*., **2018**, *7*, 127-131. c) Y. Y. Zhu, T. T. Yin, X. L. Li, M. Su, Y. X. Xue, Z. P. Yu, N. Liu, J. Yin, Z. Q. Wu, *Macromolecules*, **2014**, *47*, 7021-7029. d) R. Sakai, A. Nagai, Y.Tago, S.-I. Sato, Y. Nishimura, T. Arai, T. Satoh, T. Kakuchi, *Macromolecules,* **2012,** *45*, 4122-4127. e) R. Sakai, E. B. Barasa, N. Sakai, S.-I. Sato, T. Satoh, T. Kakuchi, *Macromolecules,* **2012,** *45*, 8221-8227. f) R. Sakai, N. Sakai, T. Satoh, W. Li, A. Zhang, T. Kakuchi, *Macromolecules,* **2011,** *44*, 4249-4257. g) R. Sakai, S. Okade, E. B. Barasa, R. Kakuchi, M. Ziabka, S. Umeda,

K. Tsuda, T. Satoh, T. Kakuchi, *Macromolecules,* **2010,** *43*, 7406-7411. h) R. Kakuchi, Y. Tago, R. Sakai, T. Satoh, T. Kakuchi, *Macromolecules,* **2009,** *42*, 4430-4435.

[11] a) M. N. Bhebhe, E. Alvarez De Eulate, Y. Pei, D. W. M. Arrigan, P. J. Roth, A. B. Lowe, *Macromol. Rapid Commun*., **2017**, 38, 1600450; b) B. Liu, L. Li, C. Lin, J. Zhou, Z. Zhu, H. Xu, H. Qiu, S. Yin, *Polym. Chem.,* **2014**,*5*, 372; c) N. Basescu, Z. –X. Liu, D. Moses, A. J. Heeger, H. Naarmann, N. Theophilou, *Nature*, **1987**, *327*, 403

[12] R. Rodríguez, E. Quiñoá, R. Riguera, F. Freire, *J. Am. Chem. Soc.,* **2016**, *138*, 9620.

[13] a) E. Vass, M. Hollósi, F. Besson, R. Buchet. *Chem. Rev.* **2003**, *103*, 1917-1954; b) j. Venkatraman, S. C. Shankaramma, P. Balaram, *Chem. Rev.* **2001**, *101*, 3131-3152; c) E. J. Milner-White, B. M. Ross, R. Ismanil, K. Belhadj-Mostefa, R. Poet, *J. Mol. Biol.* **1998**, *204*, 777.

[14] a) F. Freire, J. D. Fisk, A. J. Peoples, M. Ivancic, I. A. Guzei, S. H. Gellman, *J. Am. Chem. Soc.,* **2008**, *130*, 7839-7841; b) F. Freire,S. H. Gellman, *J. Am. Chem. Soc.,* **2009**, *131*, 7970-7972.

[15] a) B. López, E. Quiñoá, R. Riguera, *J. Am. Chem. Soc.* **1999**, *121,* 9724; b) V. Leiro, J. M. Seco, E. Quiñoá, R. Riguera, *Org. Lett.*, **2008***, 10 ,* 2733*;* c) R. García, J. M. Seco, E. Quiñoá, R. Riguera, *J. Org. Chem.* **2006**, *71 , 1119.*

[16] Although *ap* is the major conformer in solution, a minor synperiplanar (*sp*) conformation may be operative at the MPA residue where the NH-OMe interaction is nonexistent (ref. 14). *Sp* is transformed into *ap* by lowering the temperature and therefore, NH-OMe bonding increases and the NH undergoes a downfield shift. Analogous explanation justify why in the extended form, a downfield shifting is also observed for the same proton.

[17] B. Fernández, R. Rodríguez, A. Rizzo, E. Quiñoá, R. Riguera, F. Freire, *Angew. Chem. Int. Ed.*, **2018**, *57*, 3666.

[18] a) S. Leiras, F. Freire, E. Quiñoá, R. Riguera, *Chem. Sci*., **2015**, *6*, 246; b) K. Okoshi, S. Sakurai, J. K. Ohsawa, E. Yashima. *Angew. Chem. Int. Ed.,* **2006**, *45*, 8173.

Playing with the beta sheet/gamma-turn equilibrium at the pendant groups of a chiral polyene framework [i.e., poly(phenylacetylene)] allows the reversible transformation from a compressed helical scaffold to a highly stretched, almost planar helical structure. This change on the secondary structure of the polymer is accompanied with a color change from yellow to red and a solution-gel transition.

Keyword: helical polymer, gel, colorimetric sensor, self-assembly, poly(phenylacetylene)

R. Rodríguez, E. Quiñoá, R. Riguera,* F. Freire*

Stimuli-Directed Colorimetric Interconversion of Helical Polymers accompanied by a Tunable Self-Assembly Process.

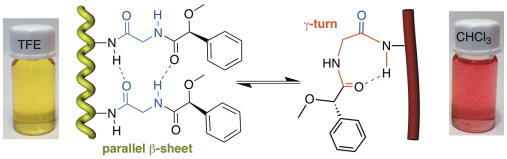

Supporting Information

Stimuli-Directed Colorimetric Interconversion of Helical Polymers accompanied by a Tunable Self-Assembly Process

*Rafael Rodríguez, Emilio Quiñoá, Ricardo Riguera and Félix Freire**

Centro Singular de Investigación en Química Biolóxica e Materiais Moleculares (CiQUS) and Departamento de Química Orgánica, Universidade de Santiago de Compostela, E-15782 Santiago de Compostela, Spain.

felix.freire@usc.es

Table of Contents

Materials and Methods

CD measurements were done in a Jasco-720. The amount of polymer used for CD measurements was 0.1 mg/mL.
UV spectra were registered in a Jasco V-630. The amount of polymers used for CD measurements were 0.1 mg/mL.
Raman spectra were carried out in a Renishaw confocal Raman spectrometer (Invia Reflex model), equipped with two lasers (diode laser 785 nm and Ar laser 514 nm).
DSC traces were obtained in a DSC Q200 Tzero Technology (TA Instruments, New Castle, UK), equipped with a refrigerated cooling system RCS90 (TA Instruments, New Castle, UK), using a Tzero low-mass aluminum pan. The heating rate used was 10 ºC/min.
TGA traces were obtained in a TGA Q5000 (TA Instruments, New Castle, UK) using a platinum pan. The heating rate used was 10 ºC/min.
GPC studies were carried out in a Waters Alliance equipped with Phenomenex GPC columns using THF as mobile phase.
AFM measurements were performed in a Park NX10 operating in non-contact mode at rt, using NCHR cantilevers.
SEM measurements were performed on a LEO-435VP electron microscope equipped with an energy dispersive X-ray (EDX) spectrometer. A drop of a solution of different polymers (0.01 mg/mL) was settled on a silicon wafer chip (Ted Pella, Inc.), and allowed to dry at rt for 12 h.
Rheology measurements were performed at 20ºC in a Rheolyst AR-1000N rheometer (TA Instruments, New Castle, UK) equipped with an AR2500 data analyzer and fitted with a Peltier plate. The storage (G') and the loss (G'') moduli were recorded at 0.1 Pa in the 0.5-50 rad/s angular frequency interval using a cone-plate geometry (diameter 4 cm, angle 2º) with solvent trap.
For molecular modeling we used Spartan 10 (MMFF94). As a molecular visualization system we used PyMOL.

Synthesis of the Monomers

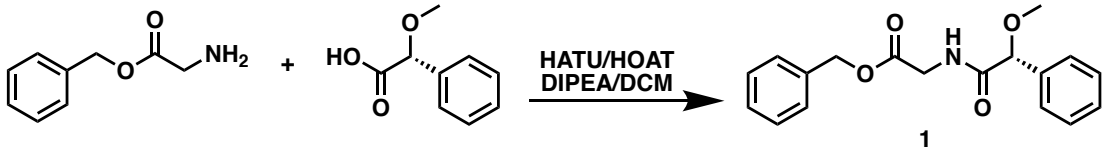

1

(2-(7-Aza-1H-benzotriazole-1-yl)-1,1,3,3-tetramethyluronium hexafluorophosphate) (HATU, 3.95 g, 1.20 equiv.), 1-hydroxy-7-azabenzotriazole (HOAT, 1.40 g, 1.20 equiv.), (*R*)-α-methoxy-α-phenylacetic acid were added (1.70 g, 1.20 equiv.) and diisopropyltriethylamine (DIEA, 1.50 ml, 1.20 equiv.) were dissolved in 80 mL of DMF, and the mixture was stirred for 15 min to activate the acid. Then, glycine benzyl ester (1.00 g, 1.00 equiv.) was added and the reaction mixture was stirred overnight. The organic layer was evaporated at reduced pressure; the crude was diluted in DCM and washed with HCl 1M, saturated solution of $NaHCO_3$ and brine. The combined organic layers were dried over anhydrous Na_2SO_4, filtered and the solvent was evaporated at reduced pressure. The crude product was chromatographed on silica gel (70-230 mesh) with hexane/ethyl acetate (6/4) as eluent [1.16 g], 86% yield of pure product.

Benzyl (*R*)-(2-methoxy-2-phenylacetyl)glycinate

^{1}H NMR (300 MHz, $CHCl_3$) δ(ppm): 3.39 (s, 3H), 4.11 (qd, J= 18.4 Hz, J= 5.6 Hz, 2H), 4.68 (s, 1H), 5.20 (S, 2H), 7.28-7.46 (m, 11H).

^{13}C NMR (75 MHz, $CHCl_3$) δ(ppm): 40.9, 57.4, 67.3, 83.6, 127.2, 128.4, 128.6, 128.7, 135.2, 136.8, 169.7, 171.0

HRMS (ESI) m/z calcd for $C_{18}H_{19}NO_4\,Na^+$ [M + Na^+]: 236.1103, found: 336.1210

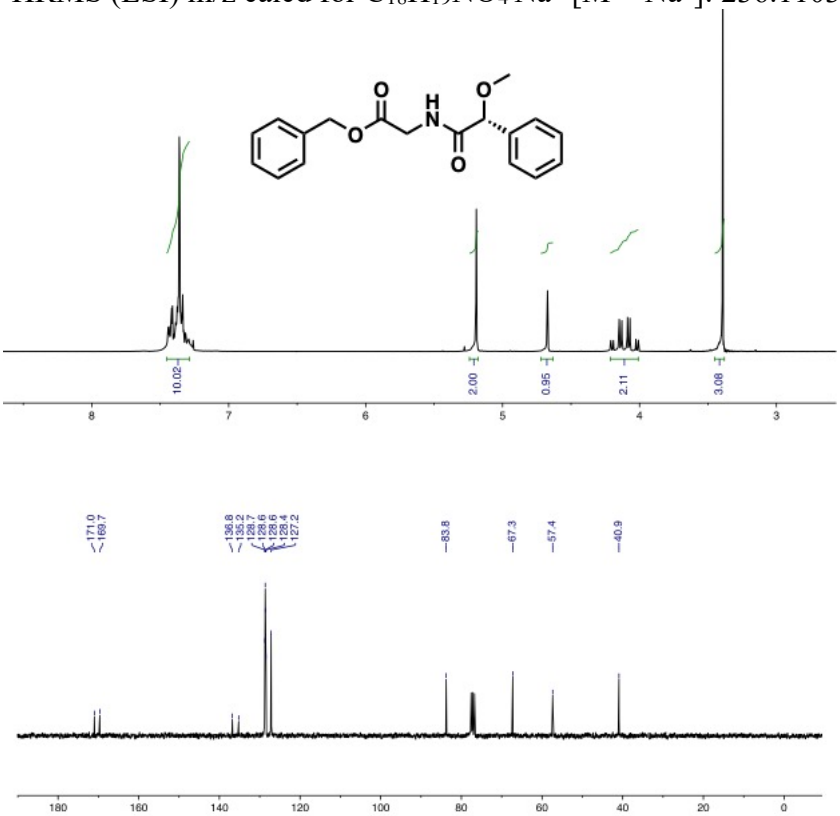

Figure S1. ^{1}H and ^{13}C NMR spectra of **1** ($CDCl_3$).

(*R*)-(2-methoxy-2-phenylacetyl)glycine (2)

Palladium carbon (0.50 g) was added to a solution of of benzyl (*R*)-(2-methoxy-2-phenylacetyl)glycinate (2.75g, 7.90 mmol) in ethyl acetate (70 ml). The reaction mixture was stirred under H_2 atmosphere for 2h. Next, the mixture was filtered over celite and the organic layers were evaporated at reduced pressure obtaining the desired compound in quantitative yield.

^{1}H NMR (300 MHz, $CHCl_3$) δ(ppm): 3.35 (s, 3H), 3.99 (qd, J= 5.7 Hz, q= 18.4 Hz), 4.70 (s, 1H), 7.28-7.41 (m, 5H), 7.51 (t, J= 5.2 Hz), 10.57 (s, 1H) .

^{13}C NMR (75 MHz, $CHCl_3$) δ(ppm): 40.9, 57.2, 83.4, 127.4, 128.6, 128.7, 136.4, 172.1, 172.3

HRMS (ESI) m/z calcd for $C_{11}H_{13}NO_4Na$ [M + Na^+]: 224.0845, found: 224.0950

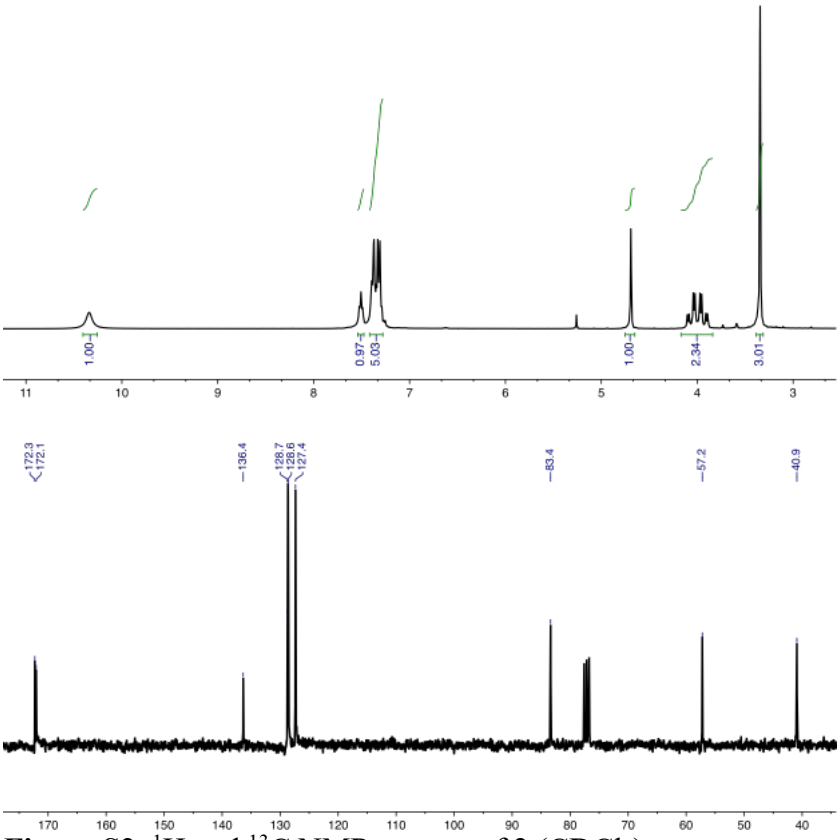

Figure S2. ^{1}H and ^{13}C NMR spectra of 2 ($CDCl_3$).

(*R*)-*N*-(2-((4-ethynylphenyl)amino)-2-oxoethyl)-2-methoxy-2-phenylacetamide (m-1)

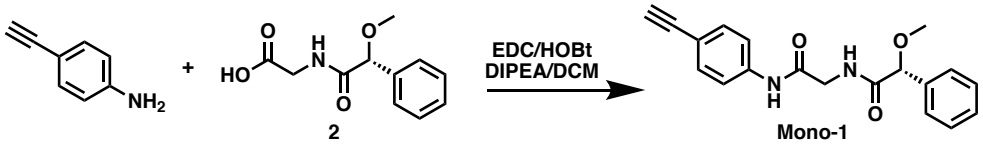

N-(3-Dimethylaminopropyl)-N′-ethylcarbodiimide hydrochloride (EDC, 3.95 g, 1.20 equiv.), 1-hydroxybenzotriazole (HOBt, 1.40 g, 1.20 equiv.), (*R*)-(2-methoxy-2-phenylacetyl)glycine acid (1.70 g, 1.20 equiv.) and diisopropyltriethylamine (DIEA, 1.5 ml, 1.20 equiv.) were dissolved in 50 mL of DCM, and the mixture was stirred for 15 min to activate the acid. Then, 4-ethynylaniline (1.00 g, 1.00 equiv.) was added and the reaction mixture was stirred overnight. The organic layer was diluted with 50 mL of DCM and washed with HCl 1M (3x50 mL). The combined organic layers were dried over anhydrous Na_2SO_4, filtered and the solvent was evaporated at reduced pressure. The crude obtained was chromatographed on silica gel (70-230 mesh) with hexane/ethyl acetate (1/1) as eluent obtaining the desired compound in 86% yield.

α_D= +30 (c= 10, $CHCl_3$).

^{1}H NMR (300 MHz, $CHCl_3$) δ(ppm): 3.05 (s, 1H), 3.35 (s, 3H), 4.18 (qd, j= 16.9 Hz, J= 5.1 Hz), 4.66 (s, 1H), 7.27 (m, 2H), 7.33 (s, 2H), 7.38 (m, 5H), (t, j= 5.1 Hz, 1H), 9.20 (s, 1H)

^{13}C NMR (75 MHz, $CHCl_3$) δ(ppm): 43.9, 57.2, 76.8, 83.6, 83.7, 117.4, 119.3, 117.7, 119.3, 127.7, 128.9, 129.0, 132.9, 136.6, 138.5, 166.6, 171.9

HRMS (ESI) m/z calcd for $C_{19}H_{18}N_2O_3$ [M + H^+]: 323.1390, found: 323.1385

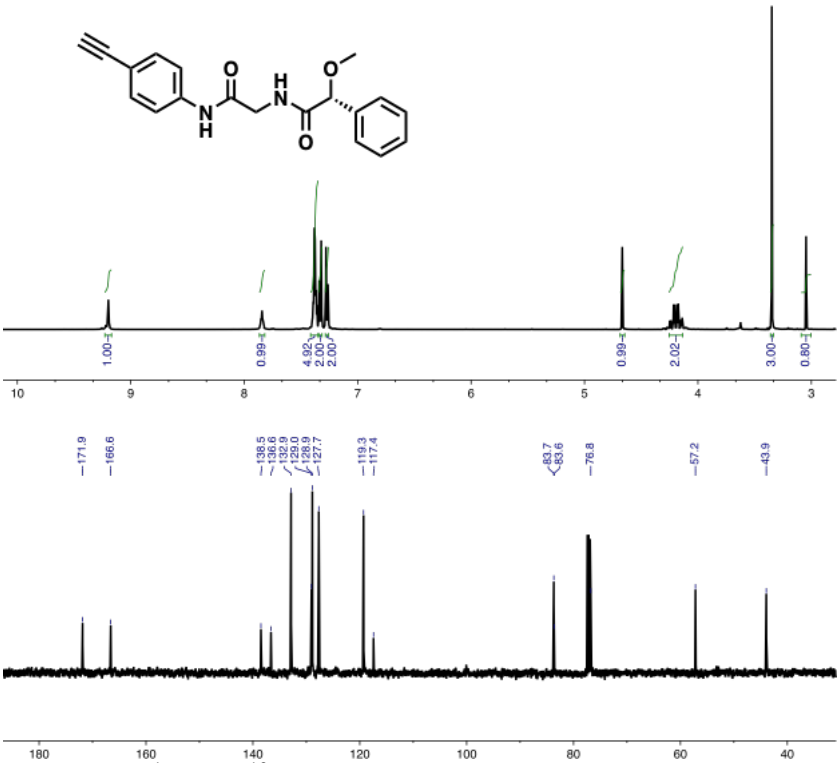

Figure S3. ^{1}H and ^{13}C NMR spectra of m-**1** ($CDCl_3$).

NMR Experiments

[1]H NMR experiments of m-1 in different solvents.

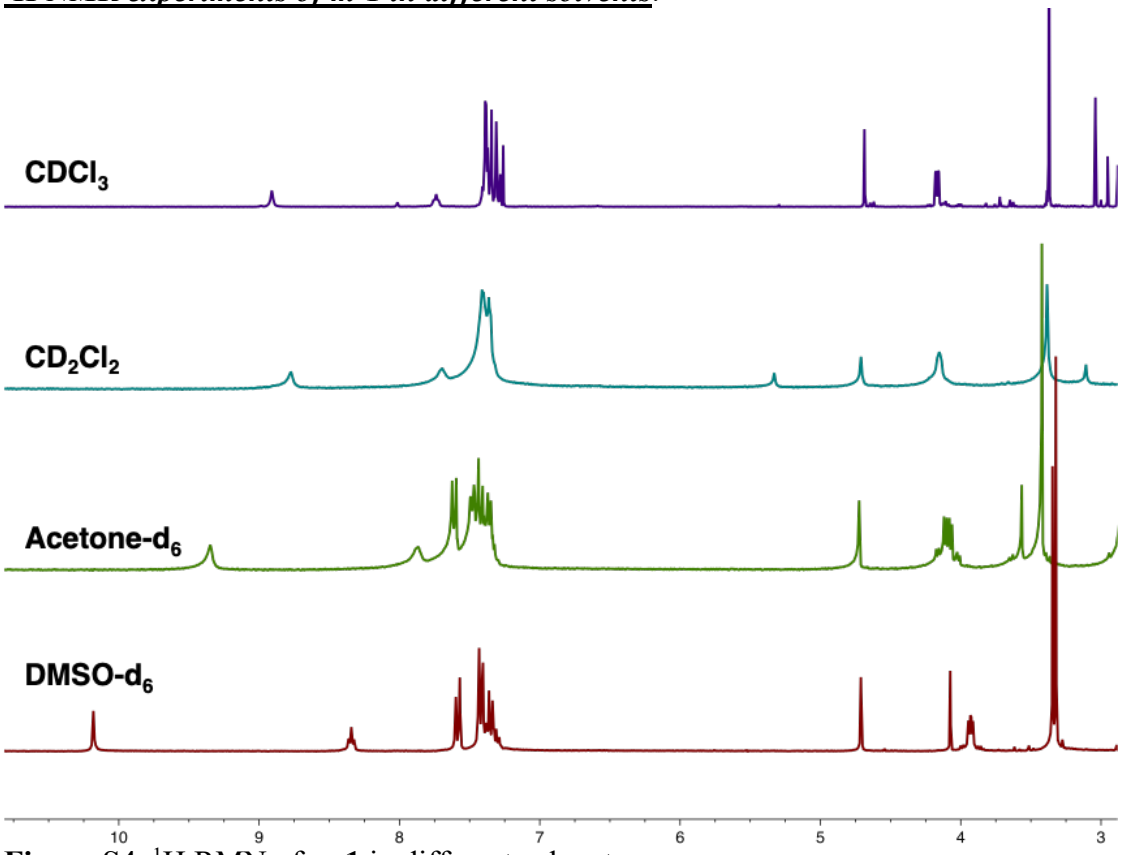

Figure S4. [1]H RMN of m-**1** in different solvents.

Conformational Studies by Circular Dichroism

For conformational studies on MPA-amides, see reference 14 in the manuscript.

a) b)

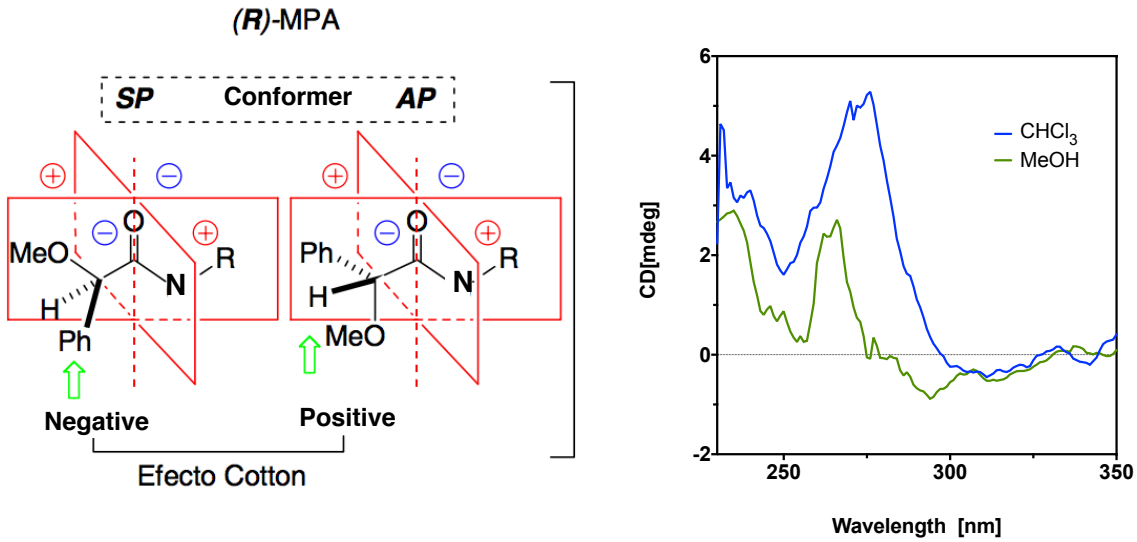

Figure S5. a) Octant rule for (*R*)-MPA amides. b) CD spectra of m-**1** in polar and low-polar solvents (CD positive= *ap* conformation) (0.3 mg/ mL).

VT-NMR Studies

VT ^{1}H NMR experiments of m-**1** in **low polar solvents** ($CDCl_3$) in the monomer indicate the presence of the gamma-turn in equilibrium with an extended structure. Remarkable changes in the anilide NH are observed as the temperature decreases, confirming equilibrium between the absence/presence of a H-bond (see figure S6). The amide proton of the Gly residue it is downfield shifted when the temperature decrease confirming the interaction of this H with the OMe group. The aromatic protons of the anilide are upfield shifted when the temperature decrease due to the aromatic shielding effect produced by the MPA on these protons in the g-form of monomer-**1**. Moreover, the glycine protons become diastereotopic when the temperature decreases as a result of different environment in those protons in the gamma-turn form.

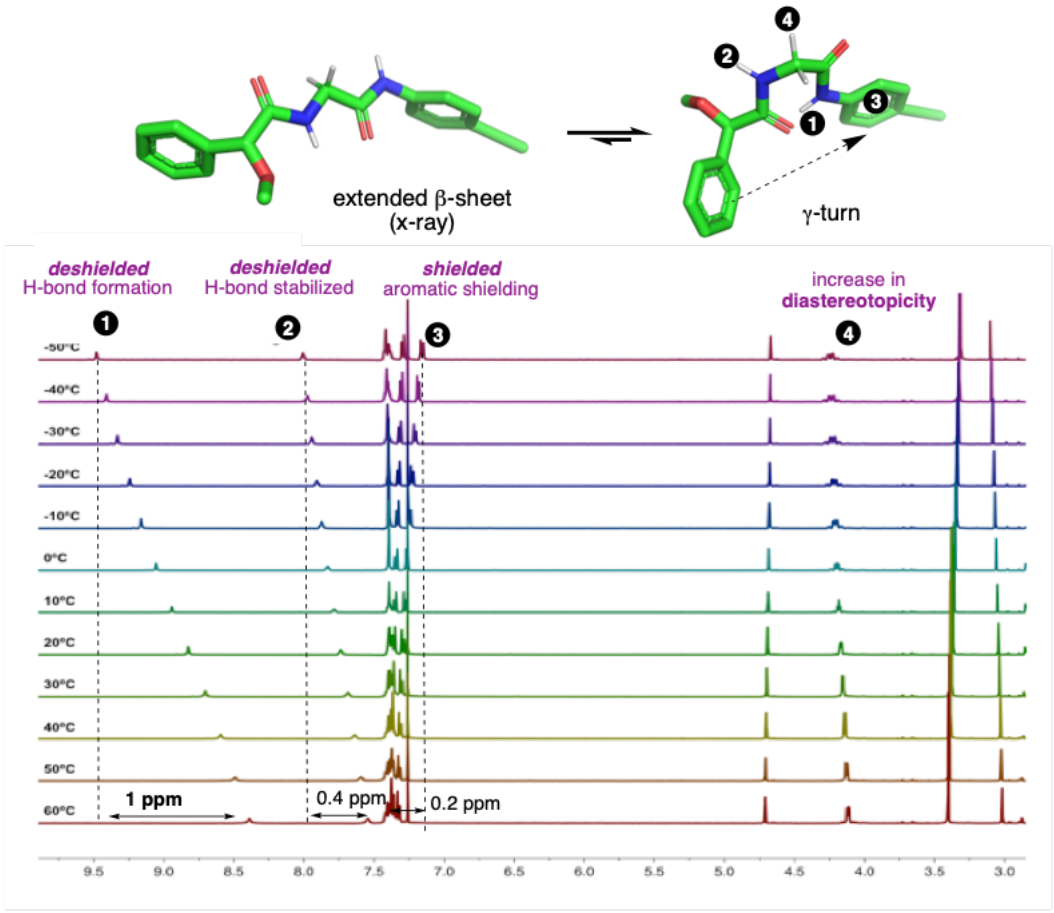

Figure S6. VT-^{1}H RMN of m-**1** in $CDCl_3$. [m-**1**]= 1mg/mL

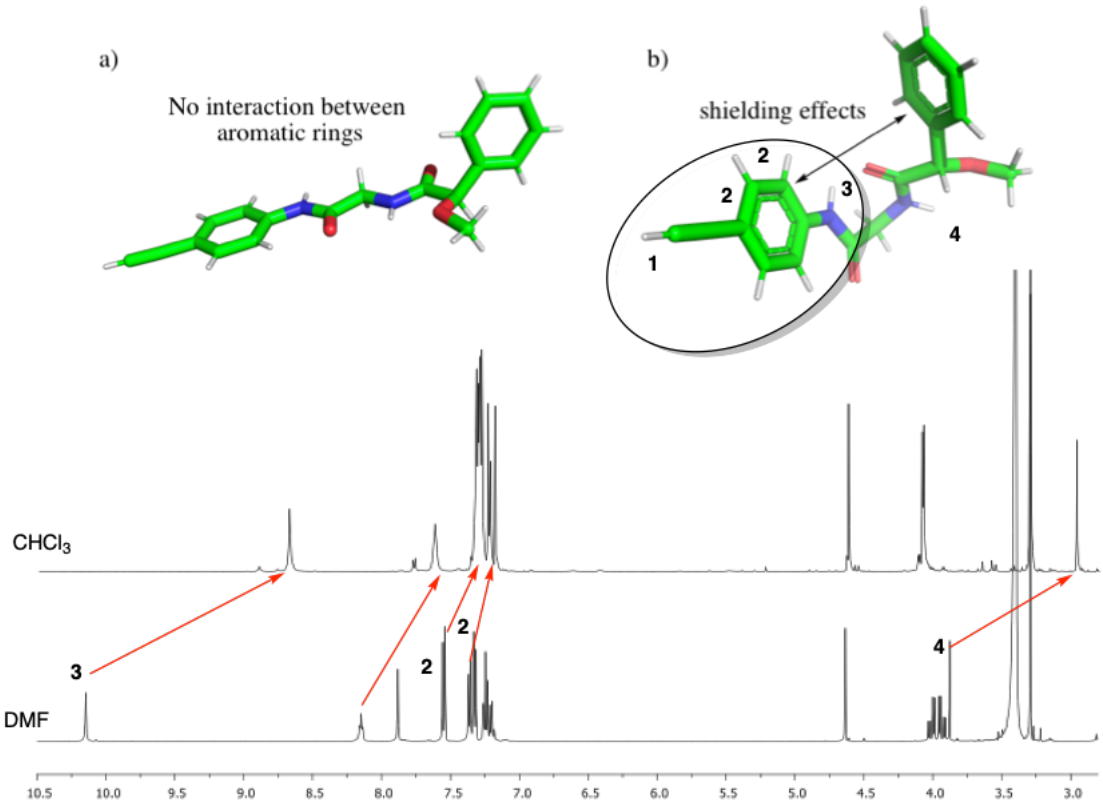

Figure S7. 3D models showing the relative position of the aromatic rings in (a) the extended and (b) the bent conformations of m-**1**. The shifts observed in NMR spectra (below) support the presence of these two different conformations. [m-**1**]= 1mg/mL

Concentration dependent NMR experiments in $CDCl_3$

In order to distinguish between conformational and aggregation effects we performed concentration dependent NMR experiments in $CDCl_3$. During these experiments only variations in the anilide NH were observed due to interaction with other molecules, but either the diastereotopicity of the Gly-CH_2 and the aromatic protons of the anilide remain constant and identical to the one observed in a diluted solution (Figure S8).

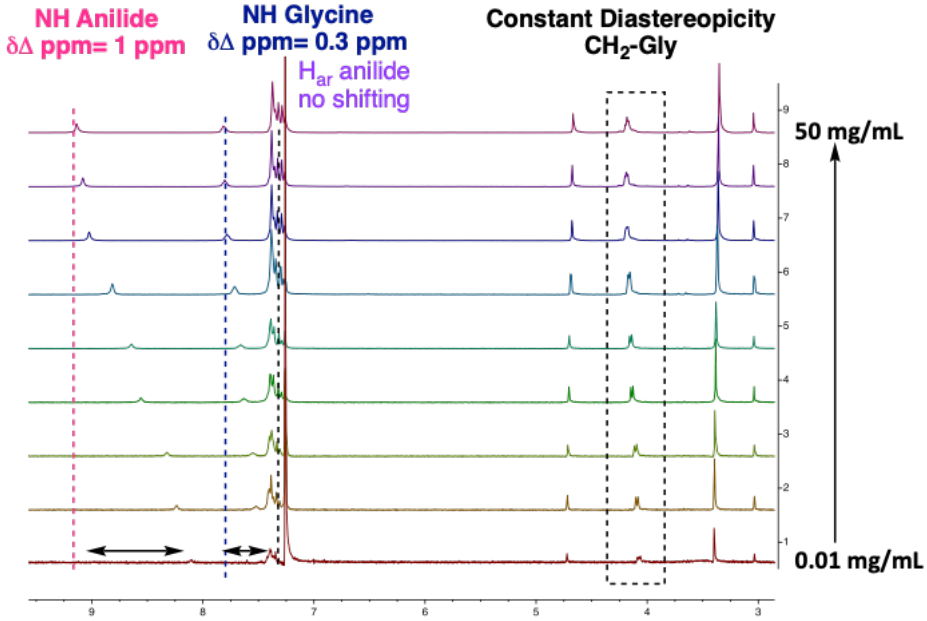

Figure S8. Concentration dependent ^{1}H RMN of m-**1** in $CDCl_3$.

VT ^{1}H NMR experiments of m-**1** in **polar solvents** (DMF-d_7) showed only variations in both amides NHs due to interaction with DMF. In addition, the diastereotopicity of the Gly-CH_2 remains constant, which clearly indicates that no conformational change takes place with the temperature (Figure S9).

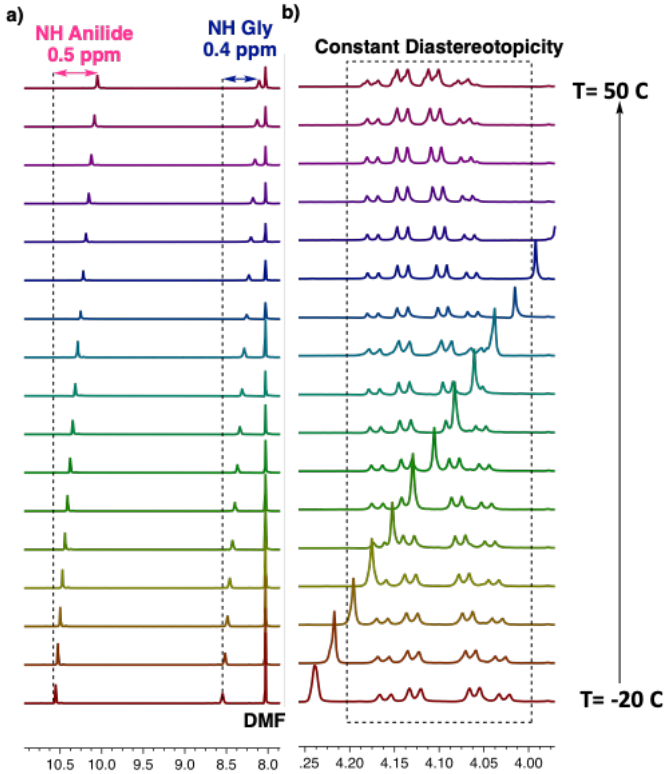

Figure S9. VT ^{1}H RMN of m-**1** in DMF-d_7. [m-**1**]= 1mg/mL

Concentration dependent NMR experiments in DMSO-d_6

Concentration dependence NMR experiments in DMSO-d_6 show no aggregation for m-**1**.

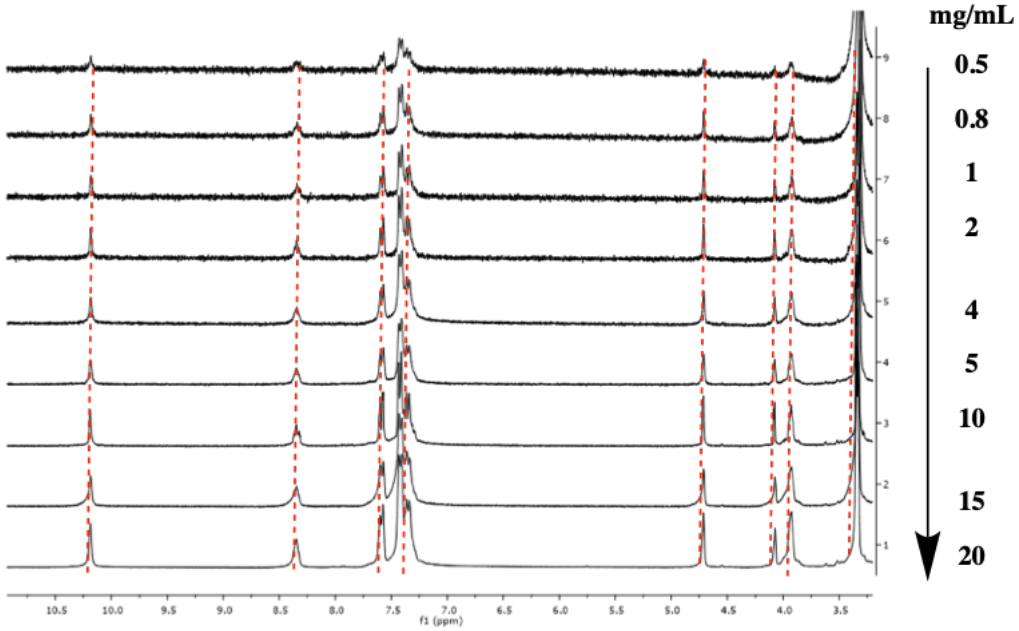

Figure S10. Concentration dependent ^{1}H-NMR studies for m-**1** in DMSO-d_6.

VT ^{1}H NMR experiments of poly-**1**

^{1}H NMR experiments of poly-**1** in low-polar ($CDCl_3$) and polar solvents (polar solvents like DMSO-d_6) display remarkable changes in their spectra, the most important feature is the absence of vinylic proton (5.6-5.8 ppm) now hidden behind the aromatic region. Also taking a look into the CH_2 Gly is clearly remarkable the different diastereotopicity in polar and low polar solvents, these results are in perfect agreement with the NMR observations for the different conformations in the monomeric species. These results clearly corroborate that this two different conformations (β-sheet and γ-turn) in the pendant groups are the responsible for the adoption of the two different polyene states (helical and planar respectively).

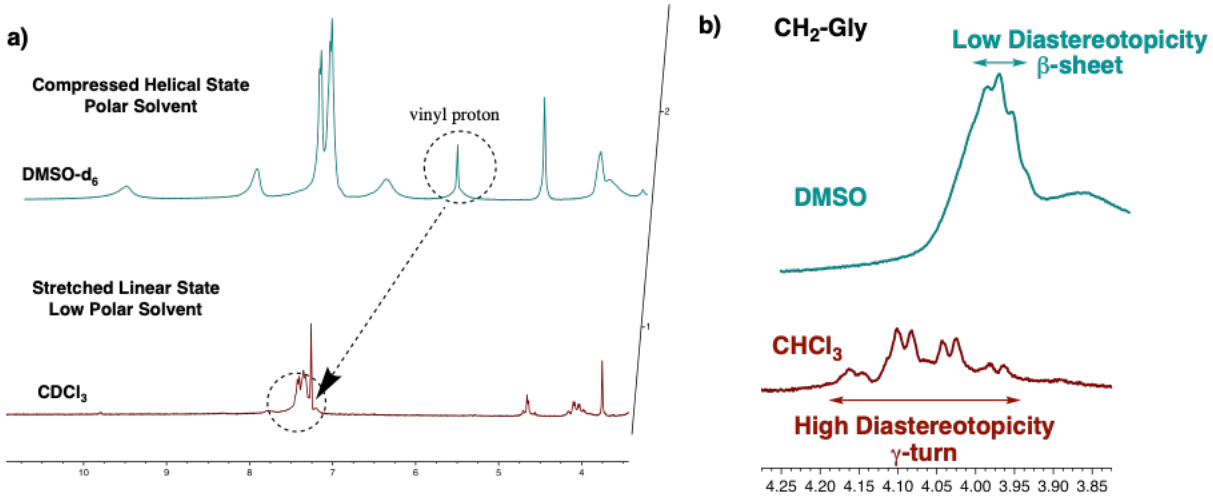

Figure S11. a) Comparison of the ^{1}H RMN of poly-**1** in $CDCl_3$ and DMSO-d_6. b) Magnification of the CH_2-Gly region showing different diastereotopicity due to different conformation of the glycine fragment.

The conversion between stretched and compressed structures followed by ^{1}H-NMR is shown below (Figure S11). As the amount of DMSO increases, the signal of the vinylic proton appears in the classical region (5.6-5.8 ppm).

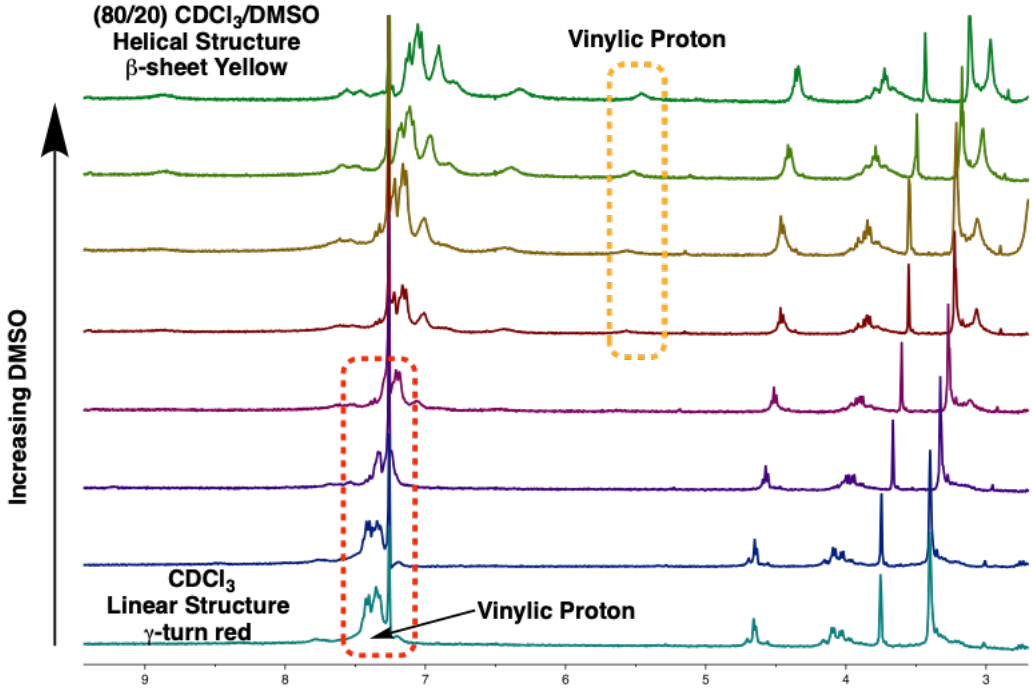

Figure S12. Conversion between stretched and compressed structures followed by ^{1}H RMN.

Synthesis of the polymers

General procedure for polymerization

The reaction flask (sealed ampoule) was dried under vacuum and argon flushed for three times before monomer was added as a solid. Then, the flask was evacuated on a vacuum line and flushed with dry argon (three times). Dry THF was added with a syringe and then triethylamine was added dropwise via syringe. A solution of rhodium norbornadiene chloride dimer, $[Rh(nbd)Cl]_2$, in THF was added at 30° C. The reaction mixture was stirring at 30°C for 6 h. Then, the resulting polymer was diluted in DCM and it was precipitated in a large amount of methanol, reprecipitated in hexane and centrifuged again.

Table S1. Polymerization conditions for poly-**1**.

Polymer	Monomer (mg)	Monomer (mmol)	$[Rh(nbd)Cl]_2$ (mg)	THF (ml)	Et_3N (µl)	Yield (%)
Poly-1	100	0.26	1.3	0.6	5	94

GPC Experiments

The molecular weight (Mn) of all polymers was estimated by GPC with THF as eluent at flow rate 1 mL/min at concentration 0.5 mg/mL using narrow polystyrene standards (PSS) as calibrants.

Different size polymers were prepared to evaluate the dependence of the dynamic behavior of poly-**1** with the polymer size, and no relationship was found. Poly-**1** dynamic properties are the same for the different lengths of the polymer chain.

Table S2. GPC data.

Polymer	Mn	PDI
Poly-**1**	20.000	1.18
Poly-**1**	79.000	2.25
Poly-**1**	380.000	2.08
Poly-**1**	2.000.000	2.48

IR experiments for Poly-1

IR experiments have been extensively used for different peptide motifs. These experiments display the presence of the turn in the case of the polymer adopting the stretched planar conformation as inferred by the small band appearing around 1759 cm^{-1}. On the other hand, the polymer adopting the compressed helical state displays the typical broad carbonyl band for a parallel □-sheet array of the pendant groups. For detailed explanation of IR experiments of these structures see references S1.

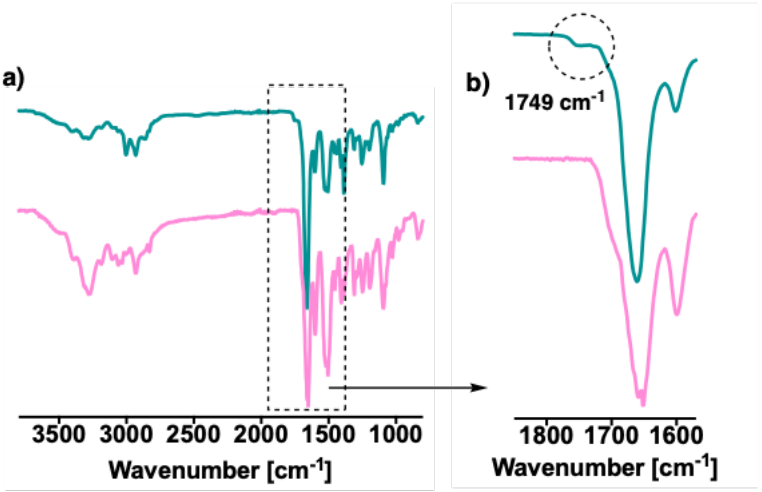

Figure S13. a) Overlay of the IR spectra of poly-**1** in both helical compressed and stretched linear state (pink and green respectively). b) Magnification of the carbonyl region.

DSC and TGA experiments

TGA experiments were performed in order to determine the thermal stability of the poly-**1** in the different states. These studies reveal a small increase in the thermal stability when comparing the linear state with the helical state.

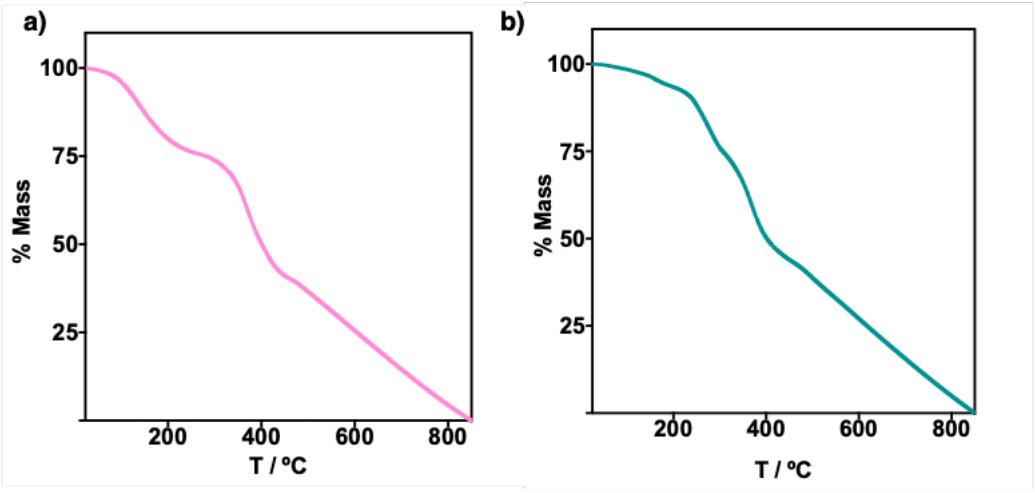

Figure S14. a) TGA trace of poly-**1** in the compressed helical state. b) TGA trace of poly-1 in the stretched helical state.

Additional CD and UV experiments

UV experiments in low-polar and polar solvents display clear differences in the UV and CD spectra. The addition of chemicals that disrupt hydrogen bonds like TFA or TBAF provoke the disruption in the □-turn (stretched linear polymer) in the pendant groups favoring the adoption of the □-sheet like structure related with the compressed helical state (figure S15c). VT-CD experiments of poly-**1** show the reversible unfolding/refolding of poly-**1** VT-CD experiments showing the reversible unfolding/refolding of poly-**1** by disruption of the □-sheet structure within pendant groups in poly-**1** (Figure S15d).

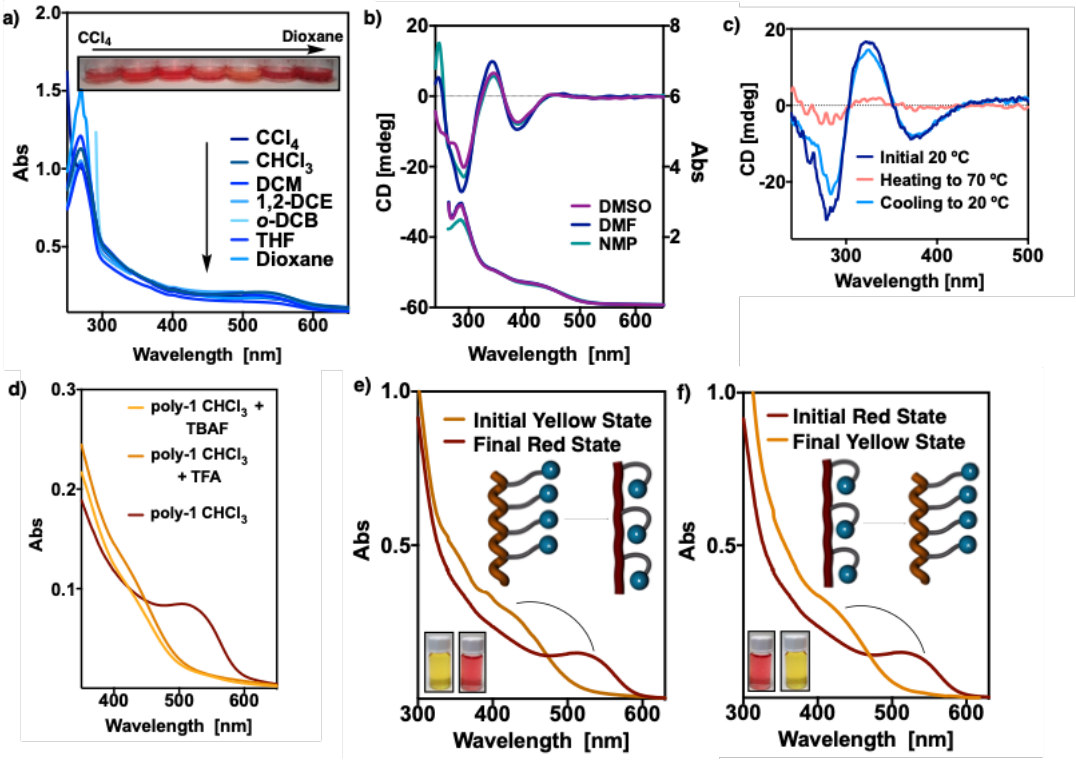

Figure S15. a) Absorption spectra of poly-**1** in the stretched linear state (0.5 mg/mL in the corresponding low-polar solvent), inset picture showing the deep red color of the solution. b) CD and UV spectra of poly-1 in the compressed helical state (0.5 mg/mL in the corresponding polar solvent). c) UV spectra of poly-**1** before and after the addition of hydrogen bond disruptors (TFA and TBAF). d) VT-CD experiments of poly-**1** (0.1 mg/ml in TFE). e) and f) reversible stretching/compressing process monitored by UV, including inset pictures of colorimetric changes and cartoon representations of polymer state.

Fluorescence experiments

Due to the great difference in the absorption spectra of poly-1 in polar and low-polar solvents —410 nm and 530 nm respectively— we tested if there is also a change in the emission spectra. Fluorescence experiments were performed in $CHCl_3$ and DMSO as representative examples of low-polar and polar solvents and the results are depicted below (see Figures S16a and S16b respectively). Also, it is remarkable that the emission of poly-**1** in the compressed helical state displays an emission 7.5 times higher than the corresponding stretched state (see Figure S16c).

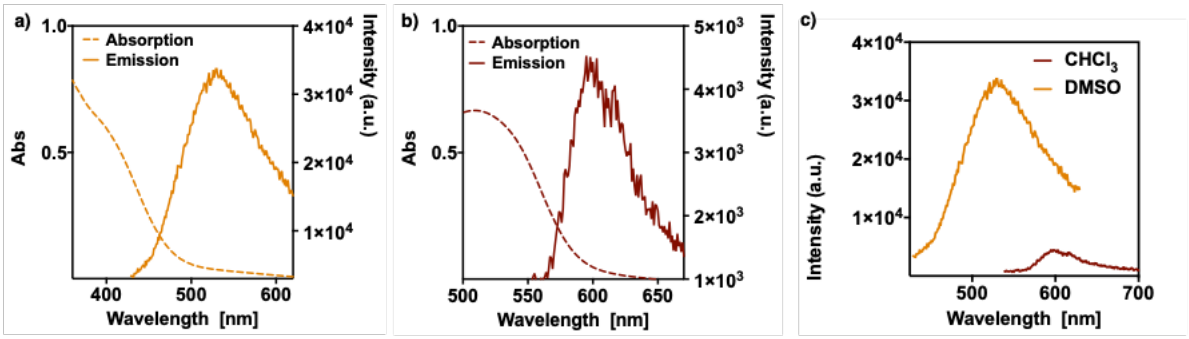

Figure S16. a) Absorption and emission spectra (dashed and continuous lines respectively) of poly-**1** in the compressed helical state (0.5 mg/mL DMSO). b) Absorption and emission spectra (dashed and continuous lines respectively) of poly-**1** in the stretched linear state (0.5 mg/mL $CHCl_3$) c) Comparison of the emission of poly-**1** in the compressed helical and the linear state (0.5 mg/mL in $CHCl_3$ or DMSO) clearly indicates that the linear state is much less emissive than the compressed helical state.

Comparison with *ortho*-MPA derivative

We have previously reported the secondary structure of a PPA bearing the anilide of the MPA acid in the *ortho*- position as pendant group. This PPA presents a polyene backbone with a ω_1 angle between conjugated double bonds of 175º that results in an almost planar helical structure. Poly-1 adopts a more conjugated polyene backbone in low polar solvents as inferred by UV-Vis and Raman experiments. Comparison of the UV-Vis of *o*-MPA and poly-**1** reveals a bathochromic shift from 508 to 530 nm, indicating a higher degree of conjugation in the case of poly-1 in low polar solvents (see Figure S17a). Raman experiments also show a blue shift in the *cis* C-H band in the Raman spectra when comparing poly-**1** with *o*-MPA. This result is also in fully agreement with the results obtained in UV experiments (Figure 17b-c). These data altogether and the absence of a Cotton effect in the CD spectra of poly-1 in low polar solvents (stretched planar structure), clearly indicates the presence of a fully conjugated planar polyene backbone with a dihedral angle between conjugated double bonds $\omega_1 = 180º$. For further details on the structure of o-MPA polymer, see Ref. 11 in main the manuscript.

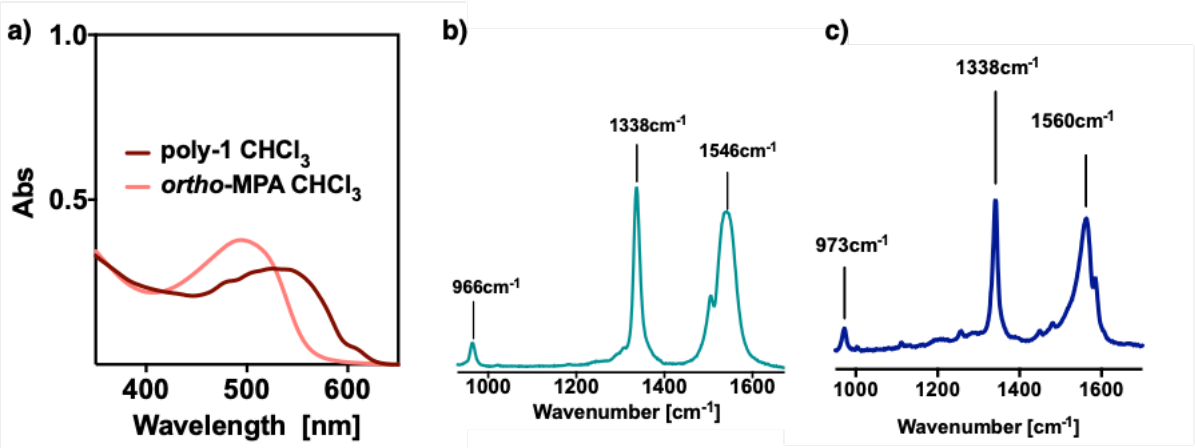

Figure S17. a) Overlay of the UV-Vis of poly-**1** in and *o*-MPA polymer showing a bathochromic shift in the case of poly-**1** (both polymers in $CHCl_3$, c= 0.1 mg/mL). b) Raman spectra of poly-**1** in the stretched linear state. c) Raman spectra of *o*-MPA polymer.

Additional SEM images

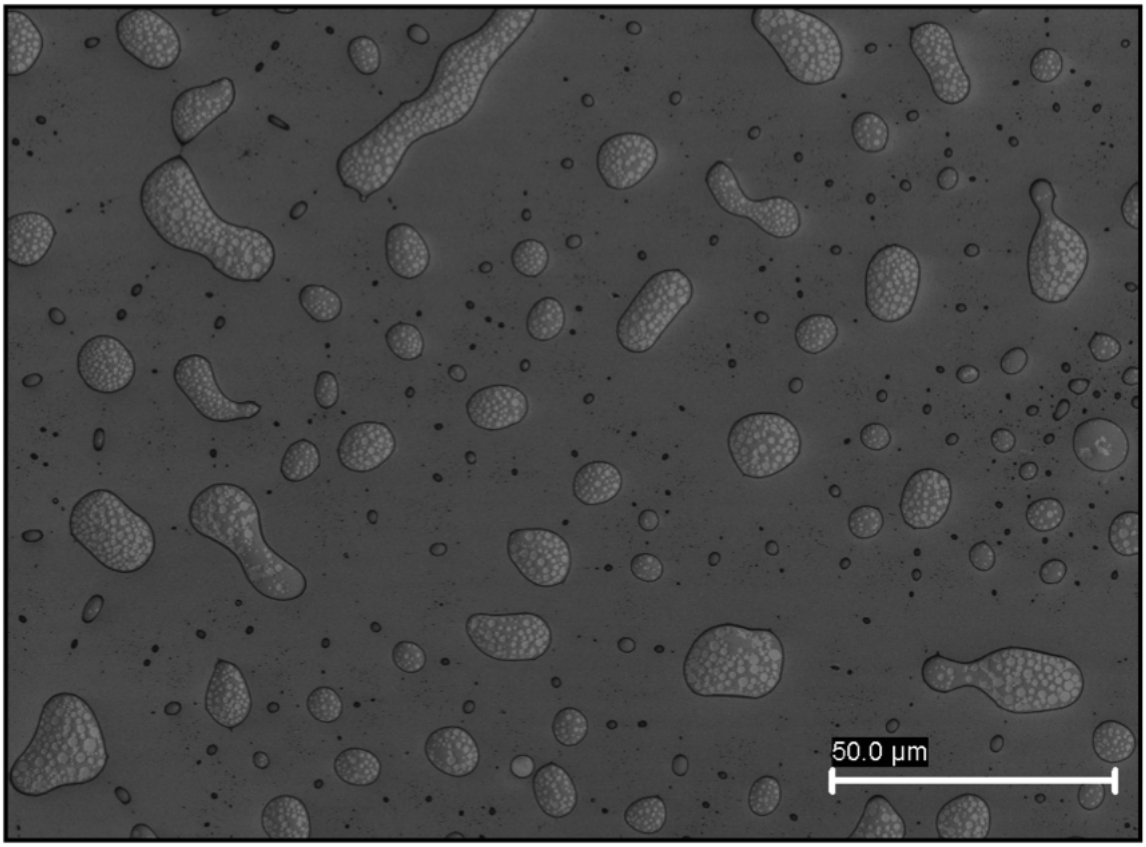

Figure S18. SEM image of the gel generated by poly-**1** in $CHCl_3$ using silicon wafer as substrate (scale= 50 µm).

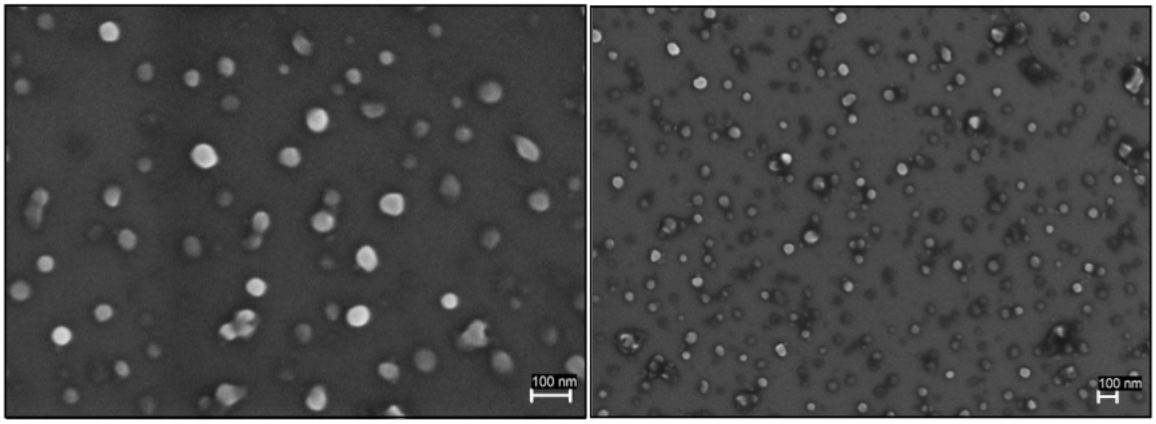

Figure S19. SEM image of the polymeric particles generated by poly-**1** in DMSO using silicon wafer as substrate (scale=100 nm).

AFM images

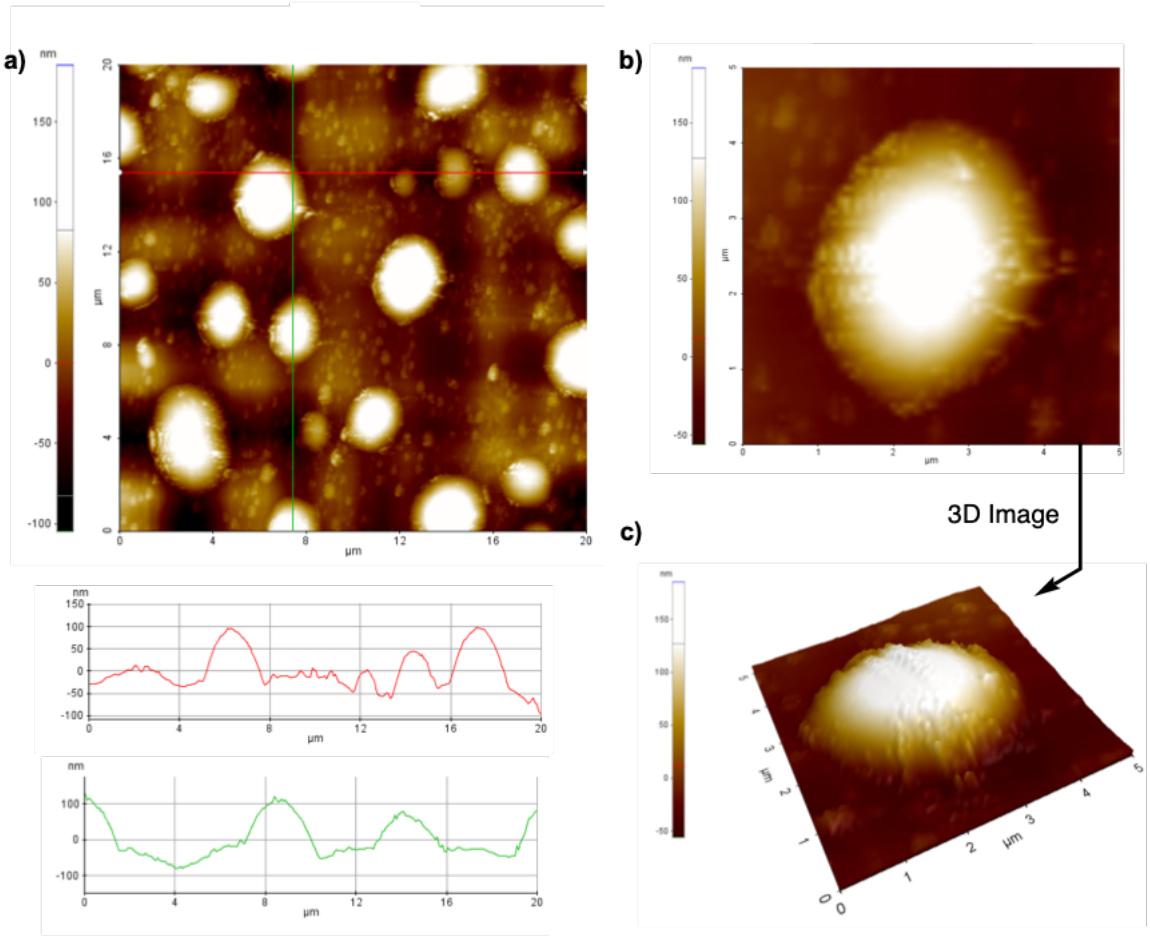

Figure S20. AFM images of the gel formed by poly-**1** in $CHCl_3$ (Substrate = silicon wafer). a) Large-scale AFM image and cross section profiles. b) Magnification of image and a). c) 3D-projection of image (b).

Poly-(R)-1 and Poly-(S)-1: Enantiomer comparison

In order to demonstrate that the conformational equilibrium in poly-(*R*)-**1**, it is due to the combination of the achiral gly residue with the chiral (*R*)-MPA moiety, we prepared the corresponding enantiomeric form, poly-(*S*)-**1**, which bears (*S*)-MPA as chiral fragment. As expected the equilibrium between an extended and a compressed helical structure still occurs in low-polar and polar solvents respectively (see Figure S21), although the helical sense adopted by poly-(*S*)-**1** is as expected opposite to the one observed in poly-*(R)*-**1**.

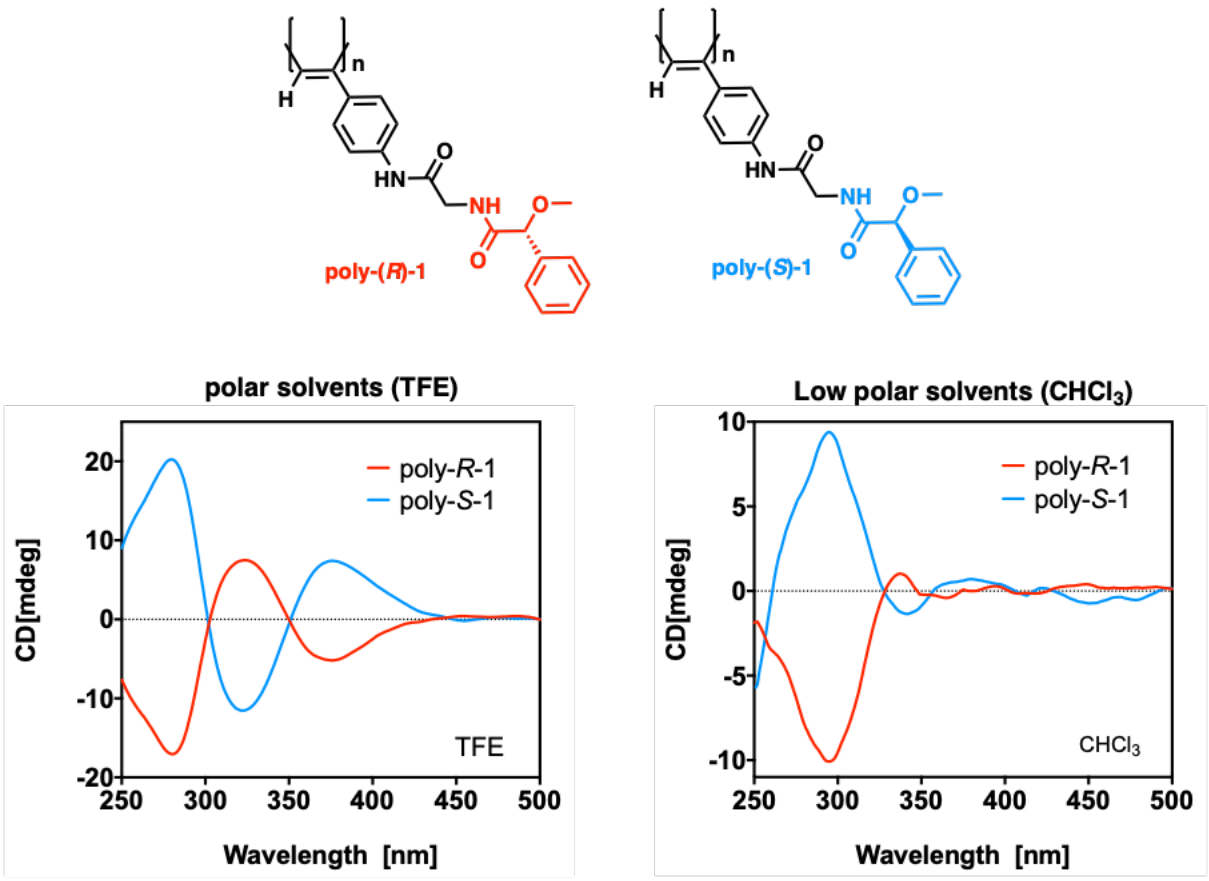

Figure S21. CD spectra comparison of poly-(*R*)-**1** and poly-(*S*)-**1** in polar and low-polar solvents.

Suporting references

[S1] a) R. Noreen, M. Moenner, Y. Hwu, C. Petibois. *Biotechnol. Adv.* **2012**, *30*, 1432-1446; b) V. Bobroff, H. H. Chen, S. Javerzat, C. Petibois. *TrAC - Trends Anal. Chem.* 2016, *82*, 443-456.